A Spectroscopic Comparison of HED Meteorites and V-type Asteroids in the Inner Main Belt

Nicholas A. Moskovitz [a,b], Mark Willman [a],
Thomas H. Burbine [c], Richard P. Binzel [d], Schelte J. Bus [e],

[a] *Institute for Astronomy, 2680 Woodlawn Drive, Honolulu, HI 96822 (U.S.A)*

[b] *Carnegie Institution of Washington, Department of Terrestrial Magnetism, 5241 Broad Branch Road, Washington, DC 20008 (U.S.A)*

[c] *Departments of Geology and Physics & Astronomy, Bates College, Lewiston, Maine 04240 (U.S.A)*

[d] *Department of Earth, Atmospheric, and Planetary Sciences, Massachusetts Institute of Technology, Cambridge, MA 02139 (U.S.A)*

[e] *Institute for Astronomy, 640 North A'ohoku Place, Hilo, HI 96720 (U.S.A)*

Number of pages: 27
Number of tables: 6
Number of figures: 11

arXiv:1003.2580v1 [astro-ph.EP] 12 Mar 2010

Proposed Running Head:
Comparison of V-type Asteroids and HED Meteorites

Please send Editorial Correspondence to:

Nicholas A. Moskovitz
Carnegie Institution for Science
Department of Terrestrial Magnetism
5241 Broad Branch Road
Washington, DC 20008, USA.

Email: nmoskovitz@dtm.ciw.edu
Phone: (202) 478-8862

ABSTRACT

V-type asteroids in the inner Main Belt ($a < 2.5$ AU) and the HED meteorites are thought to be genetically related to one another as collisional fragments from the surface of the large basaltic asteroid 4 Vesta. We investigate this relationship by comparing the near-infrared ($0.7-2.5\ \mu m$) spectra of 39 V-type asteroids to laboratory spectra of HED meteorites. The central wavelengths and areas spanned by the 1 and 2 μm pyroxene-olivine absorption bands that are characteristic of planetary basalts are measured for both the asteroidal and meteoritic data. The band centers are shown to be well correlated, however the ratio of areas spanned by the 1 and 2 μm absorption bands are much larger for the asteroids than for the meteorites. We argue that this offset in band area ratio is consistent with our currently limited understanding of the effects of space weathering, however we can not rule out the possibility that this offset is due to compositional differences. Several other possible causes of this offset are discussed.

Amongst these inner Main Belt asteroids we do not find evidence for non-Vestoid mineralogies. Instead, these asteroids seem to represent a continuum of compositions, consistent with an origin from a single differentiated parent body. In addition, our analysis shows that V-type asteroids with low inclinations ($i < 6°$) tend to have band centers slightly shifted towards long wavelengths. This may imply that more than one collision on Vesta's surface was responsible for producing the observed population of inner belt V-type asteroids. Finally, we offer several predictions that can be tested when the Dawn spacecraft enters into orbit around Vesta in the summer of 2011.

1 Introduction

The basaltic howardite, eucrite and diogenite meteorites (HEDs) and the large Main Belt asteroid 4 Vesta have traditionally been linked due to their spectroscopic similarity and the lack of any other large asteroid with the characteristic spectral signature of magmatic basalts (McCord et al., 1970; Consolmagno and Drake, 1977). The presence of a collisional family associated with Vesta supports this link. Vesta-family members, often referred to as the Vestoids, are spectroscopically classified as V-types and are dynamically linked to Vesta. The term non-Vestoid refers to any V-type asteroid that originated on a parent body other than Vesta.

The Vestoids extend from the ν_6 secular resonance at the inner edge of the Main Belt to the 3:1 mean motion resonance with Jupiter at 2.5 AU (Fig. 1, Binzel and Xu, 1993). These resonances act as a dynamical escape hatch from the Main Belt and can transport fragments removed from the surface of Vesta (or one of the Vestoids) to the Earth as HED meteorites (Gladman et al., 1997). Resolved images of Vesta reveal a large crater (~ 460 km in diameter) on its south pole (Thomas et al., 1997), supporting a scenario of collisional formation for the Vesta family.

Hydrocode simulations of the collision that formed the Vesta family (Aphaug, 1997) suggest that km-size fragments would have been removed with ejection velocities (Δv) of no greater than approximately 0.6 km/s. Simplified versions of Gauss's equations can be used to quantify the distance from Vesta in orbital element space corresponding to this ejection velocity (Zappala et al., 1996). [1] The maximum range of semi-major axes for collisionally-produced fragments can be estimated by assuming that a hypothetical Vestoid was ejected with a 0.6 km/s velocity vector aligned exclusively in a direction tangential to its orbit (Equation 4 in Zappala et al., 1996). This calculated range is $2.23 - 2.49$ AU, centered on the semi-major axis of Vesta (2.36 AU). Similar calculations can be done for both eccentricity and inclination, producing ranges of $0.06 - 0.13$ and $4.8 - 7.9°$ respectively. This region of orbital element space is enclosed by the ellipse in Figure 1.

Figure 1 shows numerous V-type asteroids in the inner Main Belt with values of Δv much larger than 0.6 km/s, some with values in excess of 2 km/s. When these objects were first discovered (e.g. Binzel and Xu, 1993; Burbine et al., 2001; Florczak et al., 2002; Lazzaro et al., 2004; Alvarez-Candal et al., 2006) it

---

[1] The following calculations assume that the true anomaly and argument of perihelion at the time of formation of the Vesta family were equal to those calculated by Zappala et al. (1996). However, these authors did not consider the effects of orbital migration due to the Yarkovsky force (Bottke et al., 2006). Therefore, the calculations presented here are approximations accurate to $\sim 20\%$.

was unclear how they could have reached such orbits. However, recent progress in the use of numerical integrators has helped to clarify this issue. Carruba et al. (2005) showed that three-body and weak secular resonances could lead to the migration of some Vestoids to orbits with $\Delta v > 0.6$ km/s. Nesvorný et al. (2008) showed that a combination of these resonances and the Yarkovsky effect could disperse the orbits of Vestoids to nearly the full extent of the inner Main Belt. However, these authors found that the observed number of V-type asteroids at low inclination ($i < 6°$) was too large to be explained by their model of Vestoid migration.

Three possibilities exist to explain this over-abundance of low-i V-types. First, these objects could be fragments of basaltic crust from a non-Vestoid differentiated parent body. In this case these objects could be spectroscopically distinct from the Vestoids, as is the case for non-Vestoid V-types in the outer Main Belt (e.g. Lazzaro et al., 2000; Moskovitz et al., 2008b). Second, they may be from Vesta, but were removed from the surface before the Late Heavy Bombardment (LHB), before the primary family forming collision, and were scattered to their current orbits as mean motion and secular resonances swept through the Main Belt during the LHB (Gomes, 1997). In this case these objects would represent an older population of Vestoids, removed from a different region on Vesta's surface and thus might be spectroscopically distinct. Third, these objects may have been ejected from the Vesta parent body at the time of family formation and have since migrated to their current orbits by some unexplored dynamical mechanism. In this case these objects should not appear spectroscopically different from other V-type asteroids in the inner Main Belt.

A similar line of reasoning motivated Hiroi and Pieters (1998) to investigate the visible-wavelength spectral features (namely the slope and 1 μm band depth) of 20 V-type asteroids in the inner Main Belt as a function of their orbital elements. These authors found that V-type asteroids with large values of Δv tended to have steeper spectral slopes than V-types with smaller Δv. However, the largest value of Δv considered by these authors was 0.65 km/s, very close to the expected ejection velocity of Vestoid fragments. Furthermore, all of the objects that were studied have since been incorporated into the Vesta dynamical family as detection completeness has increased in the last decade. Thus it is surprising that this spectroscopic trend was observed as a function of orbital parameters for objects that plausibly originated at the same time from the same parent body.

Duffard et al. (2004) attempted a similar investigation into the spectroscopic diversity of Vestoids at NIR wavelengths. This study produced unexpected results: the Band II to Band I area ratios and the Band I and Band II centers for the majority of the V-types in their sample did not agree with those of the HEDs (Band I and II refer to the 1 and 2 μm absorption bands common to

basaltic material, see §2 for definitions of these parameters). Although it has been suggested that band area ratios are sensitive to variations in grain size, temperature and space weathering (Ueda et al., 2002), band centers should be less sensitive to these effects and thus comparable between genetically related populations (i.e. the HEDs and Vestoids).

In light of recent advances in dynamical simulations (Carruba et al., 2005; Nesvorný et al., 2008) and improvements in NIR spectroscopic instrumentation (Rayner et al., 2003), we revisit the issue of the diversity of basaltic asteroids by measuring the NIR spectral properties of 39 inner Main Belt V-type asteroids. The goals of this study are threefold: (1) address the reported spectro-dynamical correlation amongst V-type asteroids in the inner Main Belt (Hiroi and Pieters, 1998) by extending our analysis out to NIR wavelengths and by including V-types across a wider range of orbital element space; (2) address the findings of Duffard et al. (2004) to look for spectroscopic differences between inner belt V-type asteroids and HED meteorites; (3) determine if any of the V-type asteroids in the inner Main Belt have spectroscopic properties suggestive of a non-Vestoid mineralogy. It is important to note that we do not attempt to extract detailed mineralogical information for individual asteroids. Instead we characterize our relatively large data set using band analysis techniques (e.g. Cloutis et al., 1986) with the intent of making statistically significant statements about the gross spectral properties of V-type asteroids relative to those of the HED meteorites.

2 Spectral Band Analysis

The reflectance spectra of minerals contain absorption features that are diagnostic of properties such as composition, albedo, grain size and crystal structure. A variety of analytic tools have been developed to interpret such information from remotely obtained spectra (e.g. Sunshine et al., 1990; Hiroi et al., 1993; Shkuratov et al., 1999; Lawrence and Lucey, 2007). Band analysis techniques (e.g. Cloutis et al., 1986) are useful for characterizing spectral data and can be used as a starting point for deriving mineralogical information (Gaffey et al., 2002). As a characterization tool, band analyses are completely objective, requiring no knowledge or assumptions about mineralogy, and can be implemented quickly for a large number of spectra. The primary goal of this work is to use band analysis techniques to facilitate a comparison between HEDs and V-type asteroids. We perform this band analysis with attention to the following parameters: the minima and central wavelength of the 1 and 2 μm olivine-pyroxene absorption features (Band I and II respectively) and the ratio of areas within these two bands. These key parameters are depicted in Figure 2. We also measure the Band I slopes of the asteroids for comparison to results of Hiroi and Pieters (1998).

Measurement of these parameters is dependent on several polynomial fits to actual data (Fig. 2). These fits include a fourth order fit to the reflectance peak at $\sim 0.7\ \mu m$, third order fits to the reflectance troughs and peak at $\sim 0.9,\ 2.0$ and $1.4\ \mu m$, and a second order fit to the red-edge of the $2\ \mu m$ band. The band minima are equal to the minima of the third order fits across each of the reflectance troughs ($0.82 - 1.03\ \mu m$ for Band I and $1.65 - 2.2\ \mu m$ for Band II). The Band I center is measured by first fitting a line (labelled Band I Slope in Fig. 2) that intersects the fitted peak at $\sim 0.7\ \mu m$ and is tangent to the reflectance peak at $\sim 1.4\ \mu m$. This continuum slope is then divided into the data and the minimum of this slope-removed band is defined as the band center. Band I centers are typically at longer wavelengths than Band I minima because of the positive Band I slope for most HEDs and V-type asteroids. Band II centers are defined as equal to the Band II minima (without dividing out a continuum slope), because the red edge of the $2\ \mu m$ band is typically unresolved in NIR telescopic data (e.g. Fig. 2). We define the red edge of the $2\ \mu m$ band to be at $2.44\ \mu m$ (the reddest wavelength for which all of our data are reliable). Band areas are calculated as the area between the band slopes and data points. The calculation of error bars for each of these band parameters is discussed in §4.

We have intentionally been very explicit in our definition of these band parameters because other studies have employed different methodologies. For instance, Cloutis et al. (1986) define the red edge of Band II at $2.4\ \mu m$ while Gaffey et al. (2002) define it at $2.5\ \mu m$. In some studies, the band centers are defined as the wavelength at which the band areas are bisected (e.g. Binzel et al., 2009). Although these differences are subtle, they do make it difficult to compare measurements from one study to another (a similar discussion of this issue was also presented by Duffard et al., 2006). We apply our methodology to all of the data considered here so that comparisons can be made between the asteroids and meteorites. These measurements are internally consistent and are not meant to be directly compared to previous works.

3   Band Analysis of HED Meteorites

To build a comparison database for the asteroids we perform a spectral band analysis for each of the HED meteorites that are included in the Brown RE-LAB spectral catalog (Pieters and Hiroi, 2004). All samples that were analyzed are listed in the Appendix. We safely ignore error bars in the measurement of the meteorite band parameters, because they are much smaller than those associated with the asteroidal data (§4), and they become irrelevant in our statistical approach to characterizing the overall spectral properties of the HEDs. The range of HED band parameters roughly agree (within $\sim 10\%$) with those measured by previous investigators (Duffard et al., 2005).

This set of HED spectra excludes some of the data that are available in the RELAB database. We do not include samples that have been processed in laser irradiation experiments. When multiple spectra for a single sample exist, which is true for about 40% of the samples, we choose data corresponding to the smallest available grain size (for RELAB this is $25\mu m$). This approach is reasonable because the grains that compose the regoliths of Vestoids are believed to be $< 25\mu m$ in size (Hiroi et al., 1994, 1995). We note that preferentially selecting these small-grained samples does not have a significant effect on any of our results. When relevant (e.g. §6), we discuss the implications of this selection criterion. Our aim in analyzing these meteoritic spectra is not to perform a detailed study of spectral changes as a function of particle size, irradiation level and other variables; for such a study see Duffard et al. (2005).

A plot of BI center versus BII center for the HEDs is shown in Figure 3. The three HED subgroups are well defined (although they do overlap) in this parameter space. The regions occupied by each subgroup have been shaded or outlined so that they can be compared to the band parameters of the V-type asteroids in §4. In general, eucrites tend to have band centers at longer wavelengths than the diogenites, which implies that they are more Fe-rich and have Ca/Mg abundance ratios much greater than 1 (Burbine et al., 2001). This is confirmed by chemical analyses of eucrite samples (Lodders and Fegley, 1998). The diogenites have shorter wavelength band centers due to Ca/Mg abundance ratios much less than 1 and relatively Fe-poor compositions. Unsurprisingly, the howardites (brecciated mixes of eucrites and diogenites) have band centers that are intermediate to that of the eucrites and diogenites. The compositional trend represented by the band centers is consistent with the origin of the diogenites at greater depths within the HED parent body, i.e. low-Ca diogenites crystallized and settled before high-Ca eucrites as the HED parent body cooled (Ruzicka et al., 1997).

A plot of BAR versus BII center is shown in Figure 4. Traditionally, BAR is plotted versus BI center due to the mineralogical relevance of this particular combination of axes (Gaffey et al., 1993). However, we are not attempting to draw mineralogical inferences from our data. Furthermore, we find that the BII centers of the three HED subgroups are better segregated with less overlap than the BI centers. Thus, the axes in Figure 4 are the preferred method for presenting our data.

The BARs do not clearly segregate the three HED subgroups, however the diogenites do tend towards larger values. The lack of high-Ca pyroxene amongst the diogenites (Burbine et al., 2001) is a likely cause for their higher BARs (Cloutis et al., 1986). Truncating the edge of BII at 2.44 μm might also have affected their BARs.

Of the 75 HEDs that were analyzed, four eucrites (Passamonte, Ibitira, NWA011,

and PCA91007) have anomalous oxygen isotope ratios. Specifically, these meteorites all have $[^{17}O/^{16}O]$ abundance ratios that are at least 0.03‰ away from the mean $[^{17}O/^{16}O]$ ratios for ordinary HEDs, which display a scatter of only $\pm$ 0.016‰ relative to their mean (Scott et al., 2009). The interpretation for these four eucrites is that they derive from unique (non-Vestoid) differentiated parent bodies. Our analysis shows that the band paramters of these four samples are in no way different from the other eucrites (Figs. 3 & 4). At face value this would seem to suggest that the spectroscopic properties (and by extension the mineralogy) of basaltic material from one parent body to the next is indistinguishable and that isotopic information is needed to distinguish individual parent bodies. However, this does not seem to be the case for all V-type asteroids in the Main Belt. For example, 1459 Magnya is a non-Vestoid V-type with distinct band parameters (Hardersen et al., 2004). Thus, while band analysis techniques are capable of distinguishing V-type asteroids with no genetic relation to Vesta, this does not seem to be the case amongst the HEDs. The reason for this remains unclear.

4 Band Analysis of V-type Asteroids

4.1 Observation & Reduction

We collected NIR spectra of 39 V-type asteroids distributed throughout the inner Main Belt (Fig. 1, Appendix A, Table 1). All of these observations, with the exception of the data of Vesta from 1981, were obtained with the SpeX instrument (Rayner et al., 2003) at NASA's IRTF. In addition to our new observations, these data include those from DeMeo et al. (2009), data from the ongoing MIT-UH-IRTF Joint Campaign for NEO Spectral Reconnaissance (NEOSR, PI's Richard Binzel & Alan Tokunaga) and the spectrum of 4 Vesta from Gaffey (1997). See the specific references for details regarding observing conditions and reduction of these data sets.

All new SpeX observations were made with the telescope operating in a standard ABBA nod pattern. SpeX was configured in its low resolution (R=250) prism mode with a 0.8" slit for wavelength coverage from $0.7 - 2.5$ μm. All targets were observed at an air mass of less than 1.5 and as near as possible to their meridian crossings. The slit was orientated along the parallactic angle at the start of each observation to minimize the effects of atmospheric dispersion. Exposure times were limited to 200 seconds. The number of exposures was selected in an attempt to obtain a consistent $S/N \sim 100$ for all asteroids. Internal flat fields and arc line spectra were obtained immediately after or before each target asteroid. A solar analog star was observed to calibrate each asteroid spectrum (i.e. solar correction, compensating for instrument response and

removal of atmospheric absorption features). Analogs were observed closely in time, altitude and azimuth to the asteroid. The spectrum of each asteroid was calibrated using a single solar analog. Specific analogs were selected as those which minimized residual atmospheric features in the calibrated spectrum of a given asteroid. Calibration and reduction of our new observations employed the Spextool package (Cushing et al., 2004).

When available, visible wavelength data from Moskovitz et al. (2008a), SMASS (Xu et al., 1995; Bus and Binzel, 2002a) or S3OS2 (Lazzaro et al., 2004) were appended to the NIR spectra to increase wavelength coverage and to improve S/N at the blue edge of the 1 μm absorption band. The addition of visible wavelength information to the NIR spectra does not significantly effect the trends in band parameters that are discussed in the following sections. Figure 11 shows that both the 1 and 2 μm absorption bands are resolved for all 49 of the spectra and that the typical S/N is either better than or comparable to previous studies of NIR band parameters of V-type asteroids (e.g. Kelley et al., 2003; Duffard et al., 2004; Hardersen et al., 2004). The targets 2653 Principia, 2851 Harbin, 3155 Lee, 3782 Celle and 4215 Kamo were each observed at two different epochs by the NEOSR program (Table 1). The data from these pairs of observations were combined into composite spectra to improve S/N and are presented as such in Figure 11. New observations of asteroids 2653 Principia and 4215 Kamo are also presented in Figure 11.

4.2   Temperature Correction to Band Centers

The band analysis procedure described in §2 was applied to each of the NIR asteroidal spectra. The results of this band analysis are summarized in Table 2. In order to compare these parameters to those of the HEDs, which were measured in a laboratory at $\sim$ 300 K, a temperature correction to the band centers was required. Temperature corrections were computed following the methodology of Burbine et al. (2009). The mean surface temperature of an asteroid (T) is approximated by the equation for energy conservation:

$$T = \left[\frac{(1 - A)L_0}{16\eta\epsilon\sigma\pi r^2} \right]^{1/4}, \tag{1}$$

where A is the albedo, L_0 is the solar luminosity (3.827×10^{26} W), η is the thermal beaming parameter (assumed to be unity), ϵ is the asteroid's infrared emissivity (assumed to be 0.9, Lim et al., 2005), σ is the Stefan-Boltzman constant and r is the asteroid's heliocentric distance. Though the albedo of 4 Vesta and 1459 Magnya are approximately 0.4 (Tedesco et al., 1990; Delbo et al., 2006), recent Spitzer observations suggest that smaller V-type asteroids may have albedos as low as 0.2 (Lim et al., 2009). Thus, the albedo of each

target was assumed to be 0.3. The calculated mean surface temperature for each of the V-type asteroids is given in Table 2. Uncertainties in the adopted parameters (A, η and ϵ) do not have a large affect on our resulting temperature corrections because of the small (1/4) exponent in Equation 1.

The temperature-dependent wavelength correction (in microns) to the BI and BII centers are given by (Burbine et al., 2009):

$$\Delta BI = (5.05 \times 10^{-3}) - (1.70 \times 10^{-5})T, \tag{2}$$

$$\Delta BII = (5.44 \times 10^{-2}) - (1.85 \times 10^{-4})T. \tag{3}$$

These equations are derived from linear fits to laboratory measured band centers for two different pyroxenes at temperatures of 293, 173 and 80 K (Moroz et al., 2000). In general these corrections are small: 0.002 μm for all of the ΔBI values (rounded to the resolution limit of the spectra) and about an order of magnitude more for ΔBII (Table 2). These shifts are much less than the range of measured band centers and thus do not have a major impact on our results, however they do improve the measured overlap of the HEDs and V-types (see §4.4). The temperature corrected band centers are presented in Table 2.

4.3   Estimated Error Bars

The spectrum of asteroid 36412 (2000 OP49) has the lowest wavelength-averaged signal-to-noise ratio (S/N~27) in this data set. This object's spectrum was used to estimate maximum statistical error bars for the measured asteroidal band parameters. Determining the error bars on band centers is non-trivial because the uncertainties for the observed data points are along the reflectance axis, not along the wavelength axis. To access the errors on the band centers of asteroid 2000 OP49 we ran a Monte Carlo simulation in which random noise (at the level of the measured signal-to-noise) was added to segments of the spectrum in the vicinity of the Band I and Band II minima. These segments were re-fit with a third-order polynomial and the new band centers were calculated. This process was repeated 100,000 times and the standard deviation of the measured band centers was calculated. The result of this error analysis gives $\sigma_{BI} = 0.003$ μm and $\sigma_{BII} = 0.011$ μm. This procedure for estimating errors on band centers is similar to that of Storm et al. (2007). Most of the asteroidal spectra are of much higher S/N (~ 100) and thus will have statistical errors for their band centers that are insignificant relative to the general trends in which we are interested.

The errors for BARs are calculated by first measuring the largest and smallest

possible band areas based on the S/N characteristics of a given spectrum. The maximum band areas are measured by subtracting noise at the 1-sigma level from each data point, while the minimum band areas are measured by adding noise at the 1-sigma level. For example, the BII area of 2000 OP49 with 1-sigma worth of noise subtracted from the data points is 0.608 and the BII area with 1-sigma worth of noise added is 0.516. We define the errors on the individual band areas to be one half of the difference between these maximum and minimum values. The net error on the BAR then involves the propagation of the errors from each band. Performing this analysis on the spectrum of 2000 OP49 gives a maximum error bar on the asteroidal BARs of $\sigma_{BAR} = 0.23$.

4.4 Band Diagrams

The asteroidal band centers are plotted in Figure 5 along with the howardite, eucrite and diogenite regions that were defined for Figure 3. Eight asteroids (4 Vesta, 956 Elisa, 1468 Zomba, 2045 Peking, 2579 Spartacus, 2653 Principia, 2763 Jeans and 4215 Kamo) were observed more than once. These individual observations are connected by the thin lines. The maximum statistical error bars calculated from the spectrum of 2000 OP49 (§4.3) are indicated in this figure and are clearly much smaller than the size of the HED regions and the range of band centers displayed by the asteroids. The variability between multiple observations of individual asteroids is typically larger than the statistical errors and is likely due to a combination of compositional variation across the surface of the asteroids, differences in observing circumstances (e.g. use of different solar analogs, different observational phase angles), and uncorrected systematic effects. Vesta is known to display large variation in its band centers due to compositional variation on its surface (Gaffey, 1997). However, such variation may not apply to these targets, which are more than an order of magnitude smaller in size. Observations of single asteroids through multiple rotation periods and with multiple instruments could determine whether any systematic effects may be inherent to these SpeX data. Note that the mean of the band centers for the V-types do not seem to be affected by the (apparently) random variability introduced by multiple observations of individual objects.

Four of the asteroids [1468 Zomba, 2823 van der Laan, 3703 Volkonskaya and 50098 (2000 AG98)] were observed on single epochs as part of the NEOSR program and do not have complementary visible wavelength data. These data have been truncated at 0.82 μm as part of the standard NEOSR reduction protocol. Thus their full 1 μm absorption feature is not resolved, thereby preventing a calculation of a BI slope and center. However, an upper limit to the BI center can be made based on the measured BI minima. The largest offset between a BI minimum and a BI center was measured to be 0.016 μm

for asteroid 7800 Zhongkeyuan. Adding this value to the BI minima of the four NEOSR asteroids produces reasonable upper limits to their BI centers. These four objects are plotted in Figure 5 as upside-down, filled triangles.

As previous authors have noted (Burbine et al., 2001), there appears to be a lack of diogenetic V-type asteroids in the inner Main Belt. However, we do find four objects that plot near the howardite-diogenite boundary in Figure 5: 2851 Harbin, 3155 Lee, 26886 (1994 TJ2) and 27343 (2000 CT102). These objects and the lack of diogentie-like asteroids are discussed in greater detail in the following section.

Our measured band centers do not span the full range of this parameter space as found by Duffard et al. (2004), instead our data suggests a good correlation between the band centers of the HEDs and V-type asteroids. This discrepancy may be due to the lower S/N of the Duffard et al. (2004) dataset and/or differences in band analysis techniques.

The dominant effect of the applied temperature corrections (§4.2) is a shift of the ensemble of asteroidal B2 centers by approximately $+0.02$ μm. This shift, though small, improves the overlap between the V-type points and HED regions in Figure 5.

A plot of asteroidal BAR versus BII center is shown in Figure 6. Only objects with fully resolved 1 and 2 μm bands can be plotted in this figure [NEOSR targets 1468 Zomba, 2823 van der Laan, 3703 Volkonskaya and 50098 (2000 AG98) are not included]. The plotted V-type asteroids have band centers that are offset from those of the HEDs by an amount that is much greater than the maximum statistical error bar. This discrepancy has been noted before (Duffard et al., 2005) and was attributed to several possible causes, including grain size, temperature, weathering and mineralogical effects. In §6 we present specific arguments for possible causes of this spectral mismatch.

5   Spectroscopic Diversity of Inner Belt V-type Asteroids

We begin this discussion by considering whether any of the inner belt V-type asteroids represent distinctly non-Vestoid mineralogies. This is facilitated by first considering the spectroscopic properties of two non-Vestoid V-type asteroids that orbit outside of the 3:1 mean motion resonance with Jupiter: 1459 Magnya and 21238 (1995 WV7). These are the only two non-Vestoid V-types with published NIR spectra. From the all-night average spectrum of Hardersen et al. (2004) we compute the band parameters of Magnya: BI center = 0.933, BII center = 1.957, and BAR = 3.395. These band centers are plotted in Figure 5 and are undistinguishable from the population of inner

belt V-types that we have analyzed. However, the BAR of Magnya is much larger than any of the objects (asteroid or meteorite) that we have measured. This large BAR is similar to the value obtained by Hardersen et al. (2004).

The second of the non-Vestoid V-types is asteroid 21238 (1995 WV7). Unfortunately a full $(0.4 - 2.5\ \mu m)$ spectrum of this asteroid does not exist in published literature. The best available data $(0.83 - 2.46\ \mu m)$ for 21238 is from the NEOSR online database (http://smass.mit.edu/minus.html). From this truncated spectrum only band minima can be measured: BI minimum = 0.906, BII minimum = 1.889. Again, an upper limit to the BI center of 21238 can be calculated by assuming the maximum offset between its BI minimum and BI center (0.016). This enables the inclusion of 21238 in Figure 5, where it falls in the lower-left corner, somewhat isolated relative to the other V-type asteroids and the only object that directly overlaps the region occupied by the diogenites.

The spectroscopic properties of these two non-Vestoid V-types (BAR for 1459 Magnya and inferred band centers for 21238) are offset from the asteroids included in our sample, thus giving credence to the dynamical arguments that these must be non-Vestoid V-types (Lazzaro et al., 2000; Michtchenko et al., 2002; Carruba et al., 2007; Roig et al., 2008). Amongst our sample of inner Belt V-types, asteroid 4038 Kristina is significantly offset with a lower BI center compared to the general HED trend (though its BII center and BAR are in no way unusual). Though this unusual BI center might imply a non-Vestoid mineralogy, that would be surprising for Kristina because it resides closer to Vesta in orbital element space $(\Delta v = 0.03\ \mathrm{km/s})$ than any other of our targets. For this reason we interpret its BI center as an indication of the mineralogical diversity inherent to members of the Vesta family and/or variability intrinsic to the observational circumstances for 4038 Kristina.

From a statistical standpoint, we find that the band centers of the HEDs and V-types are virtually indistinguishable: the mean B1 centers are 0.934 for both populations and the mean B2 centers are 1.976 and 1.987 respectively. Figure 5 confirms that the band centers of these populations are in close agreement. This is consistent with their origin on a single parent body.

It is unclear why a group of asteroids are shifted towards Band I centers that are slightly higher than those of the HEDs (Fig. 5). Amongst the HEDs, high Ca- and Fe-abundances push band centers to longer wavelengths (Burbine et al., 2001), however this should affect both Band I and Band II. This shift could be explained if we have underestimated the temperature corrections to the band centers (Equations 2 and 3). Another possibility may stem from the absence of visible wavelength data for some of these asteroids. This could be affecting the band analysis and pushing some objects towards longer BI centers. A final possibility is that this shift is a result of actual mineralogical

differences, with V-type asteroids representing a wider range of compositions than are observed amongst the HEDs.

Four objects [2851 Harbin, 3155 Lee, 26886 (1994 TJ2) and 27343 (2000 CT102)] have higher than average BARs and are offset towards smaller band centers from the majority of the asteroids in Figure 5. This apparent offset in band center is likely due to incomplete number statistics rather than the presence of non-Vesta mineralogies. Future observations of additional Vestoids would likely fill in the band center gap between these four objects and the rest of the objects studied here.

The lack of diogenite-like bodies in our sample of 39 asteroids is puzzling. This has been previously noted for V-types in the Main Belt (Burbine et al., 2001) and in the NEO population (Burbine et al., 2009). It is plausible that the four asteroids near the diogenite border in Figure 5 are primarily composed of diogenites with some eucritic material contaminating their surfaces. In general, the Vestoids are probably rubble-pile aggregates of collisional debris. The removal of large fragments from diogenetic depths ($\sim$ 10s of km) within the Vesta parent body may not have occurred. Thus, fragments of diogenite-like material on the surfaces of V-type asteroids may only be observable with high resolution surface maps and will remain undetected in the hemispherical averages provided by telescopic data. An argument that is consistent with a rubble pile model for the Vestoids is that the distribution of cosmic ray exposure ages is similar for each sub-group of the HED meteorites (Eugster et al., 2006).

Lastly, we note that the asteroid 2579 Spartacus was found to have a smaller BAR ($\sim$1.3) than the rest of our sample (Fig. 6). This has been noted before (Burbine et al., 2001) and is thought to be related to an anomalously high olivine content relative to other Vestoids. This could be due to an origin from deep within the Vesta parent body where olivine abundances were higher than in the eucritic crust, or it could be due to its origin on another parent body. If Spartacus was removed from large depths within the Vesta parent body then we would expect other diogenetic asteroids to also be present in the Main Belt, perhaps at sizes below our current observational limits.

6 Asteroidal Versus Meteoritic BARs

The band analysis of these inner belt V-types reveals a large offset in BAR between the asteroids and the HEDs (Fig. 6). It is surprising that the difference in BARs is so pronounced: the mean asteroidal BAR is 2.28 while the mean meteoritic BAR is 1.58, a discrepancy much greater than the statistical errors associated with the telescopic data. The origin of this offset is unclear, however effects related to terrestrial weathering of the meteorites, differences

between the asteroidal and laboratory environments (e.g. temperature, grain size, phase angle), instrumental systematics, the technique of band analysis, compositional differences, impacts and space weathering are potential causes. In the following we argue that composition and space weathering are the only plausible explanations for this offset, though some combination could play a role.

Weathering of Meteorites. If terrestrial weathering of the meteorites caused them to have smaller BARs, then removing found meteorites and only considering falls should reduce this offset. Of the 75 meteorite samples that were analyzed, 21 of these were observed as falls (Table 6). We find that removing found HEDs causes the regions in Figure 6 to shrink so that almost no overlap between the asteroids and the meteorites perists. Therefore it seems unlikely that terrestrial weathering is responsible for the discrepancy in BAR.

Temperature Effects. If the asteroid's low surface temperatures were the cause of their relatively large BARs, then heliocentric distance and BAR should be directly proportional. We plot these two quantities in Figure 7. Although this figure shows a significant amount of scatter (which is likely due to observational issues and compositional effects), there is a weak inverse correlation between BAR and heliocentric distance (r). The best fit to this correlation is given by:

$$\mathrm{BAR} = 3.24 - 0.44 \left(\frac{r}{1\ \mathrm{AU}} \right), \tag{4}$$

and can be interpreted as the mean spectral response of V-type mineralogies to changes in temperature. A decrease in BAR with temperature is supported by laboratory measurements of eucritic and diogenetic samples (Hinrichs and Lucey, 2002). These experiments show that the width of Band II decreases with temperature faster than the width of Band I, thus causing BAR to drop. Therefore, the asteroidal data and these laboratory measurements suggest the opposite relationship than what would be expected if temperature were the cause of the offset between the asteroidal and meteoritic BARs. The combination of Equations 1 and 4 predicts a temperature-dependent BAR trend that can be tested by future measurements of HED meteorites or remote observation of V-type asteroids (particularly those made of Vesta by the Dawn spacecraft).

It is unlikely that the increased thermal emission of the meteorites relative to the colder asteroids is a cause for the observed offset in BAR. Thermal emission from the meteorite samples causes an increase in their BII areas relative to those of the asteroids. This has the effect of producing larger BARs. If this thermal emission were accounted for then the discrepancy between the meteoritic and asteroidal BARs would increase.

Grain Size Effects. Duffard et al. (2005) showed that the BARs of eucrites and diogenites increased with grain size. The particle sizes that they investigated ranged from 25 - 500 μm. They found that large grains produced BARs up to 1.9 for eucrites and a BAR of 2.04 was measured for a single diogenite. Neither of these values is high enough to reach the mean BAR of the V-types. Furthermore, the trend between BAR and grain size for the HEDs increases quickly up 100 μm and then reaches saturation at larger grain sizes. If we ignore this saturation issue, then the large BARs of V-type asteroids might be explained by regoliths with particles beyond the upper end of the size range considered by Duffard et al. (2005). However, this contradicts the expected small regolith grain sizes ($\sim$ 25 μm) for V-type asteroids (Hiroi et al., 1994, 1995) and the general result of polarization studies which suggest that asteroid surfaces have grains less than 300 μm in size (Clark et al., 2002). Furthermore, the multi-km asteroids in our sample should have regoliths with grains smaller than that observed on the sub-km asteroid Itokawa (Masiero et al., 2009), which has particles down to at least 1 mm in size (Fujiwara et al., 2006). We note that the BAR offset persists if we consider only RELAB samples with particles greater than or equal to 1 mm in size. For these reasons we argue that grain size effects are not sufficient to explain the observed BAR offset, however the presence of coarse regoliths on the surfaces of these asteroids could be a contributing factor.

Phase Effects. The asteroidal observations were performed at phase angles (defined as the angular separation between the Sun and observer as viewed from the target) between 2° and 30° (Table 1). As was the case for heliocentric distance, the BARs of the asteroids show significant scatter as a function of phase angle. However, our observations show a weak trend of increasing BAR with phase angle (ϕ):

$$\text{BAR} = 2.17 + 0.007 \left(\frac{\phi}{1 \text{ deg}} \right). \tag{5}$$

Telescopic observations of near-Earth V-type asteroids across a wide range of phase angles would be an important test for the validity of Equation 5. Furthermore, future studies similar to those performed by Cloutis et al. (2007) will be essential to accurately characterize the effects of observing geometry on reflectance spectra of meteorite samples.

Very small ($< 2°$) phase angles were not accessed by our telescopic observations, thus is is not clear whether the trend of Equation 5 remains linear or turns down for $\phi < 2°$. If it turns down then asteroidal phase angles of less than 2° could result in small BARs similar to those of the HEDs. However, the effective phase angles (= angle of incidence + angle of emission) for the RE-LAB measurements were typically between 15° and 30° (Burbine et al., 2001; Duffard et al., 2005). Thus, if all else was equal, the BARs of the asteroids

and the meteorites would have been comparable due to the overlapping range of observed phase angles. For this reason it seems unlikely that phase effects could have resulted in the observed BAR offset.

Instrumental Systematics. The offset in BAR could be due to an uncorrected systematic effect inherent to the SpeX instrument or the reduction process. However, this seems unlikely because the observations of 4 Vesta from 1981 (which were not performed with SpeX) result in a BAR (2.55) that is well outside of the range displayed by the meteorites and one that is similar to the value measured from the data of Vesta obtained with SpeX. Furthermore, reduction of SpeX data with different software packages (e.g. Kelley et al., 2003) and NIR observations of V-type asteroids with other instruments (e.g. Duffard et al., 2004) also result in large BARs. Future high-S/N observations with different NIR spectrographs will help to determine whether any systematics are affecting our results.

Band Analysis Technique. The definition of the red edge of Band II at 2.44 μm acts to artificially reduce that band's area. It is apparent that the 2 μm band for many of the asteroids extends past this cutoff (Fig. 11) and for some meteorites this band can extend out past 2.6 μm. Unfortunately the asteroidal data are sharply truncated at these longer wavelengths due to absorption by atmospheric water bands. Two tests have been performed which suggest that the BAR offset is not related to our somewhat arbitrary definition for the edge of the 2 μm band.

First, we remeasured the BARs for all of the HEDs with the edge of BII defined at 2.6 μm. This redefinition had the effect of shifting the median BAR of the HEDs from 1.62 to 2.14. Although this reduced the discrepancy, the median BAR of the asteroids (equal to 2.26) with the cutoff at 2.44 μm was still larger than this redefined meteoritic BAR. It is safe to assume that increasing the cutoff wavelength for the asteroids would also increase their BARs and thus preserve the offset relative to the HEDs.

The effect of moving the edge of BII was tested for those asteroids with measured signal at wavelengths beyond 2.44 μm. Figure 8 shows how the median BARs of the meteorites and the asteroids varies as a function of the BII cutoff. All of the asteroids were included when the cutoff was defined at 2.44 μm, 39 asteroids have data long-wards of 2.48 μm, 31 asteroids could be measured with a cutoff at 2.49 μm, and 17 asteroids were included with a cutoff of 2.5 μm. Figure 8 clearly shows that the increase in BAR associated with extending the edge of BII to longer wavelengths is similar for both the asteroids and the meteorites. This suggests that if the asteroid data could be extended to longer wavelengths, then the BAR offset from the meteorites would persist.

Compositional Effects. Compositional variation can not be ruled out as a cause for the difference between the BARs of the HEDs and the V-type asteroids. However, it would be surprising if the composition of the HEDs were wildly different from these V-type asteroids, particularly due to the numerous lines of evidence that suggest a direct link between these two populations (Consolmagno and Drake, 1977; Drake, 1979; Binzel and Xu, 1993; Nesvorný et al., 2008). Making detailed statements regarding the mineralogical cause of such a large BAR offset between the HEDs and these V-types would require sophisticated spectral modeling (e.g. Lawrence and Lucey, 2007; Shkuratov et al., 1999) and is beyond the scope of this work.

Impact Effects. The Vesta family is probably several billions of years old (Bottke et al., 2005), thus its members have experienced significant collisional evolution over their lifetimes. Impacts onto the surfaces of V-type asteroids would result in shock heating and the production of impact glass. The build-up of significant quantities of impact-generated material would affect reflectance spectra. We consider the results of two previous studies to investigate these effects, however further work should be done to better understand the spectroscopic implications of impacts on the surface of V-type asteroids.

Burbine et al. (2001) included a spectrum of impact glass from the eucrite Macibini in their analysis of HED meteorites. A band analysis of this spectrum reveals a BAR of 1.77. This BAR is smaller than all but one of the V-type asteroids (2579 Spartacus), thus suggesting that the addition of impact glass to unshocked HED material would not result in the large BARs seen for asteroids.

Adams et al. (1979) measured the effects of high pressure (597 kbar) shock on the reflectance spectrum of enstatite pyroxene. We found the BAR of their shocked and unshocked enstatite spectra equal to 2.09 and 2.36 respectively. Thus, the BAR of this sample decreased following shock. This result also suggests that impact-induced alteration can not produce the large BARs of V-type asteroids.

Space Weathering Effects. Space weathering (i.e. modification of surfaces by micro-meteorite impact heating and irradiation by high energy particles) is a final possibility for explaining the large asteroidal BARs. Unfortunately little work has been done to understand the weathering of basaltic asteroids. This is partly due to the commonly held view that Vesta and the Vestoids have fresh or pristine surfaces (Hiroi et al., 1995; Pieters et al., 2006; Vernazza et al., 2006); an assumption rooted in the spectroscopic similarity between V-type asteroids and the HEDs at visible wavelengths (McCord et al., 1970; Consolmagno and Drake, 1977; Binzel and Xu, 1993) and the assumption of lunar-style weathering (Clark et al., 2002) for asteroidal surfaces, irrespective of composition.

In general, the majority of studies on the space weathering of asteroids have focused on establishing a link between the visible wavelength spectral properties of S-type asteroids and ordinary chondrite meteorites (e.g. Wetherill and Chapman, 1988; Clark et al., 2002; Nesvorný et al., 2005; Willman et al., 2008). Space weathering on these bodies is assumed to be analogous to that which occurs on the Moon, i.e. the vaporization and redeposition of submicroscopic metallic iron by proton bombardment and/or micro-meteorite impact results in a depression of spectral absorption features and a reddening of spectral slope (Clark et al., 2002).

Two independent sets of experiments have been performed to investigate the space weathering of HED meteorites. Vernazza et al. (2006) performed ion irradiation experiments to simulate weathering by the bombardment of solar wind particles. These authors irradiated a particulate sample (10-100 μm grain size) of the eucrite Bereba at several different levels of ion fluence. We have performed a band analysis on the three samples (unaltered, moderately irradiated and heavily irradiated) shown in their Figure 1. The results of this analysis are summarized in Table 3. Though the spectra of the irradiated samples, which exhibit steep red slopes and significantly depressed absorption features, do not resemble the spectra of any V-type asteroids, the band analysis does show that the BARs of the irradiated samples are larger by about 25% relative to the unaltered Bereba sample. Qualitatively this shift is of the right magnitude and direction to potentially explain the BAR offset between the HEDs and V-type asteroids. It is worth noting that the band centers of the unaltered Vernazza et al. (2006) Bereba sample do not match those of the Bereba sample or any other of the eucrites from RELAB (Table 6). This is likely due to differences in the preparation of the samples: RELAB uses a horizontally mounted sample tray, whereas Vernazza et al. (2006) used a compacted, vertically mounted sample. Nevertheless, their results are compelling and certainly merit further investigation.

The second set of HED weathering experiments were performed by Wasson et al. (1997, 1998) who used laser irradiation to simulate weathering by micro-meteorite impacts. Although one eucrite (Millbillillie) and one diogenite (Johnstown) were originally included in this study, problems related to the intensity of the laser necessitated a second series of experiments in which only Millbillillie was studied. We will only discuss the results of this second set of experiments. Prior to irradiation Millbillillie was ground to particle sizes of < 75 μm. It was found that irradiation produced spherical blobs of glassy material that were similar in composition to the original sample and were typically > 75 μm in diameter. These investigators divided their irradiation products into two categories (fully and partially irradiated) delineated by a cutoff in particle size at 75 μm. The fully irradiated products (> 75 μm in size) contained $\sim 95\%$ of the glassy material produced by the laser irradiation, the partially irradiated material contained the remaining 5%. We have

performed our band analysis on the unaltered, partially and fully irradiated spectra (Figure 9) from the Wasson et al. (1998) study. The results of this band analysis are given in Table 4.

The spectrum of the fully irradiated material (Figure 9) does not resemble any of the V-type asteroids that were included in our survey (Figure 11). Furthermore, it does not have band centers or a BAR that are comparable to any of the meteorites and asteroids that were analyzed. This suggests that the fully irradiated sample is not a good analog for space weathered V-type asteroids, which is not terribly surprising due to the large particle sizes of this material. On the other hand the partially irradiated sample closely resembles unaltered Millbillillie material and has band centers that are typical for both the HEDs and V-type asteroids. More interesting though is that the partially irradiated sample has a BAR that is greater by $\sim 2\%$ (due to a greater decrease in the Band I area relative to Band II, see Fig. 9). This small fraction is far from explaining the $\sim 40\%$ offset between the BARs of the HEDs and V-type asteroids, however it again emphasizes the need for further study of space weathering processes on V-type asteroids.

If V-type asteroids have weathered surfaces containing submicroscopic metallic iron, then their continuum slopes should be steeper that those of the HEDs (Clark et al., 2002). We check this by comparing Band I slopes (Figure 10). This figure shows that the V-types tend to have larger Band I slopes than the HEDs[2]. Though this is consistent with the expected spectroscopic effects induced by space weathering, it is unclear why V-type asteroids still have pronounced 1 and 2 μm absorption features while weathered lunar basalts and S-type asteroids exhibit reduced band depths (Clark et al., 2002). This issue may be related to compositional differences: the spectroscopic manifestation of weathering on V-type asteroids may be different because of their lower iron and olivine abundances (Burbine et al., 2001) relative to both the ordinary chondrites and typical lunar material (Lodders and Fegley, 1998).

Expanded irradiation and proton bombardment experiments with howardite samples (which are the best analogs to Vesta's spectrum, Pieters et al., 2006) could offer insight on the spectral implications of weathering on Vesta-like surfaces. If the observed spectroscopic differences between the V-type asteroids and the HED meteorites are due to space weathering, then older, more weathered regions on Vesta's surface should have band centers similar to the HEDs, but BARs that are significantly larger. The Visible and Infrared Mapping Spectrometer (VIR-MS) onboard the Dawn spacecraft (Russell et al., 2004) will help to provide insight on this issue.

---

[2] Note that the ratio of the reflectance peaks at $\sim$1.4 μm and $\sim$0.75 μm as defined by Cloutis et al. (1986) is similarly indicative of continuum slope and shows the same trend as that of the Band I slopes in Figure 10.

A Combination of Effects. The surfaces of asteroids are complex environments that differ from laboratory samples of meteorites in multiple ways. In this section, we have shown that terrestrial weathering of the HEDs, temperature effects, phase effects, and impacts all act to increase the BAR discrepancy between the asteroids and the meteorites. Thus it is reasonable to suggest that a combination of these effects would also increase the BAR discrepancy. Furthermore, we have shown that the technique of band analysis and instrumental systematics do not have a significant impact on producing discrepant BARs. This leaves grain size, composition and space weathering to explain the asteroidal BARs. Although some of these cannot individually explain the BAR offset, further work is required to understand the spectroscopic effects from a combination of these factors.

7 Band Parameters and Orbital Properties

7.1 Comparison to Hiroi and Pieters (1998)

Hiroi and Pieters (1998) found that V-type asteroids outside of the Vesta family tended to have steeper spectral slopes at visible wavelengths than V-types within the family, a trend that was attributed to an enhancement of weathered material on the surfaces of non-family members. At the time of their study the dynamical boundaries of the Vesta family extended to $\Delta v \sim 0.5$ km/s. However, more recent definitions of the family (Nesvorný et al., 2008) now incorporate all of the Hiroi and Pieters (1998) asteroids and include members out to $\Delta v \sim 1$ km/s. Thus, it is surprising that this spectro-dynamical trend exists for V-types that can all be linked to the same collisional origin.

Hiroi and Pieters (1998) measured "visible redness" (roughly analogous to $V - R$ color) and Band I depth (defined as the difference in reflectance between the peak at ~ 0.75 μm and the Band I minimum) for each of their targets using the Modified Gaussian Model (MGM, Sunshine et al., 1990). Ideally, we would do the same for all 39 asteroids observed here, however application of the MGM to such a large data set is impractical. Furthermore, our spectra do not include visible wavelength data for each asteroid, thus precluding the measurement of visible redness for some objects. However, it was shown in the previous section that the difference in Band I slope between V-type asteroids and HED meteorites may be linked to the effects of space weathering (Fig. 10). In addition, it is believed that the production of submicroscopic metallic iron via space weathering has spectral implications that are in some ways similar at visible and NIR wavelengths (Clark et al., 2002). Therefore we use Band I slope as a proxy for visible redness.

22

The results of Hiroi and Pieters (1998) suggest that V-types with $\Delta v > 0.5$ km/s should tend to have large Band I slopes. The mean Band I slope for V-types with $\Delta v > 0.5$ km/s is 0.79 while the mean for V-types with $\Delta v < 0.5$ km/s is 0.70, a shift of approximately 10%. This trend is consistent with the Hiroi and Pieters (1998) result, however it is not as pronounced: the objects that they referred to as non-Vesta family members showed $\sim 20\%$ higher mean visible redness than objects within the Vesta family.

Though this shift in Band I slope is consistent with Hiroi and Pieters (1998), there are several reasons to suggest that it is not a significant result. First, the probability associated with the two-sided KS statistic suggests that the distributions of Band I slopes for V-types with Δv on either side of 0.5 km/s are unlikely ($< 1\sigma$) to be derived from distinct parent populations. Second, variations in Band I slope of ± 0.1 (similar in magnitude to the 10% offset) are seen with multiple observations of the same asteroid (Table 2). Finally, the subset of 28 V-types with $\Delta v > 0.5$ km/s have Band I slopes distributed across the full range of values shown by the HEDs and other V-types, with an excess of only a few objects at large values. This is in contrast to Hiroi and Pieters (1998) who show that 7 out of 8 of their non-Vesta family members have visible redness greater than that of the HEDs and other V-types. For these reasons we interpret the difference in Band I slopes for V-types with Δv on either side of 0.5 km/s as a consequence of low number statistics.

Our inability to convincingly reproduce at NIR wavlengths the results of Hiroi and Pieters (1998) may be related to the assumed equivalence between visible redness and Band I slope. It could also be related to the sensitivity of NIR spectra to slope variations, particularly at the endpoints of the spectra. Unfortunately, only seven of our targets (4 Vesta, 1929 Kollaa, 2442 Corbett, 3155 Lee, 3657 Ermolova, 4038 Kristina, and 4215 Kamo) are shared in common with Hiroi and Pieters (1998), and of these seven objects none have $\Delta v > 0.5$ km/s. NIR observations of the V-type asteroids that Hiroi and Pieters (1998) categorize as "non Vesta family" objects are needed to better address this issue.

7.2 Spectral Implications of Nesvorný et al. (2008)

The dynamical simulations performed by Nesvorný et al. (2008) did not produce a sufficient number of Vestoid fragments with low inclination orbits to explain the observed distribution of V-type asteroids in the inner Main Belt. They concluded that the inner Main Belt may contain V-type asteroids from non-Vestoid parent bodies or fragments from the surface of Vesta that were ejected at an epoch earlier than the main family-forming collision. In either case it is reasonable to suggest that the regions of orbital element space under-

populated in the Nesvorný et al. (2008) simulations may contain V-types that are spectroscopically distinct from "ordinary" Vesta family members.

The under-populated region in the Nesvorný et al. (2008) simulations was referred to as Cell 2 and defined as: $2.32 < a < 2.48$, $0.05 < e < 0.2$, $2° < i < 6°$. This region was chosen to be diagnostic of the number of V-types at low inclinations. Table 5 lists the median band centers and BARs for V-type asteroids in four different dynamical regions: inside Cell 2, outside of Cell 2, inclinations less than 6° and inclinations greater than 6°. Note that all but three of the objects studied here have orbital eccentricities between 0.05 and 0.2, thus the region labelled as "Outside Cell 2" in Table 5 actually includes those eccentricities spanned by Cell 2. This is done to increase the number statistics within that region and does not affect any of the following conclusions. Eleven objects are included in Cell 2, 33 objects orbit outside of Cell 2, 22 have inclinations less than 6° and 23 have inclinations greater than 6°.

The median values of the band centers for objects in Cell 2 and with $i < 6°$ are at longer wavelengths than the band centers for objects outside of these regions (Table 5). This shift to longer wavelengths is larger than the maximum statistical error bars on the band centers and is most pronounced in the comparison of objects on either side of $i = 6°$ (the apparent difference in BAR is smaller than the statistical errors and thus may not be significant). It is important to note that this shift is subtle and may simply be a consequence of low number statistics. Nevertheless, it is interesting that the dynamical simulations of Nesvorný et al. (2008) may have an observational counterpart.

We can speculate about what it means for the interpretation of V-type asteroids in the inner Main Belt if this band center-inclination trend is real. Amongst the HEDs, the relatively Ca- and Fe-rich eucrites have band centers at longer wavelengths than the Mg-rich and Fe-poor diogenites (Burbine et al., 2001). Thus, V-type asteroids at low inclinations may be characterized as generally eucritic in composition. If these objects represent an older population of Vestoids (Nesvorný et al., 2008), then they may have come from a crater other than the one on Vesta's south pole (which is thought to have excavated down into Vesta's diognite-like upper mantle and produced the main Vesta family; Gaffey, 1997). Two depressions in Vesta's northern hemisphere, each approximately 150 km in diameter, have been interpreted as impact craters (Thomas et al., 1997). These craters may not have excavated down to Vesta's upper mantle and thus would generate fragments primarily eucritic in composition. Low-inclination V-type asteroids, with eucrite-like band centers, could have originated from one of these smaller craters. If these speculations are correct, then we expect that the Dawn spacecraft (Russell et al., 2004) will not observe large outcroppings or concentrations of diogenite-like material at the bottom of the two ~ 150 km-diameter craters.

8 Summary

We have observed and analyzed the spectra of 39 V-type asteroids. Comparison of their band parameters to those of HED meteorites from the RELAB database reveals a close correlation between band centers. We do not find the wide range of band centers that was reported by Duffard et al. (2004). We suspect that this difference is due to the lower S/N of the Duffard et al. (2004) data set. We were able to confirm an offset in BAR between the HEDs and V-type asteroids (Duffard et al., 2005) and argue that this offset is consistent with our initial understanding of space weathering effects on Vesta-like mineralogies However, further work is necessary to understand whether a combination of grain size, composition and/or weathering could be responsible for this offset. Several other possible causes were discussed and found to be unlikely. We were unable to reproduce at NIR wavelengths the spectro-dynamical association found by Hiroi and Pieters (1998), namely inner belt V-types do not show any correlation between slope across their 1 μm bands and distance from Vesta in orbital element space. We note that a search for correlation between other spectroscopic characteristics (band centers, slopes, depths and areas) and dynamical properties (semi-major axis, inclination, eccentricity, Δv) did not reveal any significant results.

We did not find any new evidence to suggest the presence of V-type asteroids with non-Vesta mineralogies [e.g. 1459 Magnya and 21238 (1995 WV7)]. Instead, the band parameters of these objects seem to represent a continuum of compositions that are consistent with an origin from a single parent body, most likely 4 Vesta. Only asteroid 2579 Spartacus is found to have a band area ratio that is significantly offset from the general trend represented by the other targets. This has been noted before (Burbine et al., 2001) and could be due to its origin on another parent body, however it could also be a large fragment that originated from greater depths (relative to the other targets) within the Vesta parent body. The lack of additional spectroscopic outliers amongst the V-type asteroids in the inner Main Belt implies that they are of a common origin. However, this does not preclude the possibility that inner belt V-types include basaltic crustal fragments from multiple differentiated parent bodies that are indistinguishable with band analysis techniques.

We have reported that V-type asteroids with low inclinations ($i < 6°$) in the inner Main Belt tend to have band centers shifted to longer wavelengths. This is compelling in light of the dynamical results of Nesvorný et al. (2008), however additional data should be obtained to confirm or refute the significance of this finding. In particular, a focused study on low-inclination V-type asteroids may provide further insight on whether these objects are spectroscopically distinct.

This study has resulted in several predictions that can be tested by the Dawn spacecraft when it enters into orbit around Vesta in the summer of 2011. First, we have parameterized the dependence between temperature and BAR (Equations 1 and 4). Spectroscopic observations with VIR-MS of regions at various temperatures on Vesta's surface can be used check this dependence. We have also suggested that fresher, less weathered surfaces on Vesta (e.g. impact craters) should have smaller BARs than the surrounding terrain. And finally, if the low inclination V-type asteroids in our study are predominantly eucritic in composition and were removed from one of the minor impact craters in Vesta's northern hemisphere (Thomas et al., 1997), then we expect that these craters will be devoid of significant quantities of diogenite-like material.

Appendix A: Asteroid Spectra

In this appendix we present the spectra of all V-type asteroids analyzed in this study. Numerical designations are shown in each panel. Some targets were observed on multiple occasions: the dates of these observations are indicated in a year, month, day format (YYMMDD) following the object designation. Observations prior to the year 2006 were either published in DeMeo et al. (2009), obtained as part of the ongoing MIT-UH-IRTF Joint Campaign for NEO Spectral Reconnaissance (NEOSR), or for the spectrum of 4 Vesta from 1981, obtained by Gaffey (1997). When available, visible wavelength data from one of several sources (Bus and Binzel, 2002a; Lazzaro et al., 2004; Moskovitz et al., 2008a) have been appended to the NIR data. Multiple NEOSR observations of 2653 Principia, 2851 Harbin, 3155 Lee, 3782 Celle and 4215 Kamo were combined into composite spectra. All spectra have been normalized to unity at 1 μm and are all presented at the same scale.

(FIGURE 11 SHOULD GO HERE)

Appendix B: HED Band Parameters

This appendix contains a table of the measured HED band parameters. The columns in this table are: name of the sample, meteorite type, mean particle size of the sample when the spectra were measured, BI and BII centers, and the ratio of BII area to BI area (BAR). The samples are listed alphabetically within each of the HED subgroups. Some samples were not ground into particles to measure their reflectance spectrum: these are indicated as "chip" in the particle size column.

(Table 6 SHOULD GO HERE)

Acknowledgements

References

Adams, J. B., Horz, F., Gibbons, R. V., 1979. Effects of shock-loading on the reflectance spectra of plagioclase, pyroxene and glass. 10th Annual Lunar and Planetary Science Conference, Houston, Texas, Abstract. pp. 1-3.

Alvarez-Candal, A., Duffard, R., Lazzaro, D., Michtchenko, T., 2006. The inner region of the asteroid Main Belt: A spectroscopic and dynamic analysis. A&A 459, 969-976.

Asphaug, E., 1997. Impact origin of the Vesta family. Met. & Planet. Sci. 32, 965-980.

Binzel, R. P. and Xu, S., 1993. Chips off of asteroid 4 Vesta - Evidence for the parent body of the basaltic achondrite meteorites. Science 260, 186-191.

Binzel, R. P., Rivkin, A. S., Thomas, C. A., Vernazza, P., Burbine, T. H., Demeo, F. E., Bus, S. J., Tokunaga, A. T., Birlan., 2009. Spectral properties and composition of potentially hazardous asteroid (99942) Apophis. Icarus 200, 480-485.

Bottke, W. F., Durda, D., Nesvorný, D., Jedicke, R., Morbidelli, A., Vokrouh-

licky, D., Levison, H. F., 2005. The Fossilized Size Distribution of the Main Asteroid Belt. Icarus 175, 111-140.

Bottke, Jr., W. F., Vokrouhlický, D., Rubincam, D. P., Nesvorný, D., 2006. The Yarkovsky and Yorp effects: Implications for asteroid dynamics. Annual Review of Earth and Planetary Sciences 34, 157-191.

Burbine, T. H., Buchanan, P. C., Binzel, R. P., Bus, S. J., Hiroi, T., Hinrichs, J. L., Meibom, A., McCoy, T. J., 2001. Vesta, Vestoids, and the howardite, eucrite, diogenite group: Relationships and the origin of spectral differences. Met. Planet. Sci. 36, 761-781.

Burbine, T. H., Buchanan, P. C., Dolkar, T., Binzel, R. P., 2009. Pyroxene mineralogies of near-Earth vestoids. Met. Planet. Sci. 44, 1331-1341.

Bus, S. J. and Binzel, R. P., 2002a. Phase II of the Small Main-Belt Asteroid Spectroscopic Survey: The observations. Icarus 158, 106-145.

Bus, S. J. and Binzel, R. P., 2002b. Phase II of the Small Main-Belt Asteroid Spectroscopic Survey: A Feature-Based Taxonomy. Icarus 158, 146-177.

Carruba, V., Michtchenko, T. A., Roig, F., Ferraz-Mello, S., Nesvorný, D., 2005. On the V-type Asteroids Outside the Vesta Family. I. Interplay of Nonlinear Secular Resonances and the Yarkovsky Effect: The Cases of 956 Elisa and 809 Lundia. A&A 441, 819-829.

Carruba, V., Michtchenko, T. A., Lazzaro, D, 2007. On the V-type Asteroids Outside the Vesta Family. II. Is (21238) 1995 WV7 a fragment of the long-lost basaltic crust of (15) Eunomia. A&A 473, 967-978.

Clark, B. E., Hapke, B., Pieters, C., Britt, D., 2002. Asteroid space weathering and regolith evolution. In: Bottke Jr., W. F., Cellino, A, Paolicchi, P. and Binzel, R. P.(Eds.), Asteroids III, Univ. of Arizona Press, Tucson, pp. 585-599.

Cloutis, E. A., Gaffey, M. J., Jackowski, T. L., Reed, K. L., 1986. Calibrations of phase abundance, composition and particle size distribution for olivine-orthopyroxene mixtures from reflectance spectra. J. Geophys. Res. 91, 11641-11653.

Cloutis, E. A., Craig, M. A., Bailey, D. T., 2007. Bidirectional reflectance properties of orthopyroxene. 38th Annual Lunar and Planetary Science Conference, League City, Texas, abstract no.1300.

Consolmagno, G. J., Drake, M. J., 1977. Composition and evolution of the eucrite parent body - Evidence from rare earth elements. Geochim. Cosmochim. Acta 41, 1271-1282.

Cushing, M. C., Vacca, W. D., Rayner, J. T. 2004. Spextool: A Spectral Extraction Package for SpeX, a 0.8-5.5 Micron Cross-Dispersed Spectrograph. PASP 116, 362-376.

Delbo, M. and 11 co-authors, 2006. MIDI observation of 1459 Magnya: First attempt of interferometric observations of asteroids with the VLTI. Icarus 181, 618-622.

DeMeo, F. E., Binzel, R. P., Slivan, S. M., Bus, S. J., 2009. An extension of the Bus asteroid taxonomy into the near-infrared. Icarus 202, 160-180.

Drake, M. J., 1979. Geochemical evolution of the eucrite parent body - Possible

nature and evolution of asteroid 4 Vesta. In: Gehrels, T. (Ed.), Asteroids, Univ. of Arizona Press, Tucson, pp. 765-782.

Duffard, R., Lazzaro, D., Licandro, J., de Sanctis, M. C., Capria, M. T., Carvano, J. M., 2004. Mineralogical characterization of some basaltic asteroids in the neighborhood of (4) Vesta: First results. Icarus 171, 120-132.

Duffard, R., Lazzaro, D., de León, J., 2005. Revisiting spectral parameters of silicate bearing meteorites. Met. Planet. Sci. 40, 445-459.

Duffard, R., de León, J., Licandro, J., Lazzaro, D., Serra-Ricart, M., 2006. Basaltic asteroids in the near-earth objects population: a mineralogical analysis. A&A 456, 775-781.

Eugster, O., Herzog, G. F., Marti, K., Caffee, M. W., 2006. Irradiation records, cosmic-ray exposure ages and transfer times of meteorites. In: Lauretta, D. S., McSween, H. Y.(Eds.), Meteorites and the Early Solar System II, Univ. of Arizona Press, Tucson, pp. 829-851.

Florczak, M., Lazzaro, D., Duffard, R., 2002. Discoveries new V-type asteroids in the vicinity of 4 Vesta. Icarus 159, 178-182.

Fujiwara, A. and 21 co-authors, 2006. The rubble-pile asteroid Itokawa as observed by Hayabusa. Science 312, 1330-1334.

Gaffey, M. J., 1997. Surface lithologic heterogeneity of asteroid 4 Vesta. Icarus 127, 130-157.

Gaffey, M. J., Bell, J. F., Brown, R. H., Burbine, T. H., Piatek, J. L., Reed, K. L., Chaky, D. A., 1993. Mineralogical variations within the S-type asteroid class. Icarus 106, 573-602.

Gaffey, M. J., Cloutis, E. A., Kelley, M. S., Reed, K. L., 2002. Mineralogy of Asteroids. In: Bottke Jr., W. F., Cellino, A, Paolicchi, P. and Binzel, R. P.(Eds.), Asteroids III, Univ. of Arizona Press, Tucson, pp. 183-204.

Gladman, B. J. and 9 co-authors. 1997. Dynamical Lifetimes of Objects Injected Into Asteroid Belt Resonances. Science 277, 197-201.

Gomes, R. S., 1997. Dynamical effects of planetary migration on the primordial asteroid belt. Astronomical J. 114, 396-401.

Hardersen, P. S., Gaffey, M. J., Abell, P. A. 2004. Mineralogy of Asteroid 1459 Magnya and Implications for its Origin. Icarus 167, 170-177.

Hinrichs, J. L., Lucey, P. G., 2002. Temperture-dependent near-infrared spectral properties of minerals, meteorites and lunar soil. Icarus 155, 169-180.

Hiroi, T., Pieters, C. M., 1998. Origin of vestoids suggested from the space weathering trend in the visible reflectance spectra of HED meteorites and lunar soils. Antartic Meteorite Research 11, 163-170.

Hiroi, T., Bell, J. F., Takeda, H., Pieters, C. M., 1993. Modeling of S-type asteroid spectra using primitive achondrites and iron meteorites. Icarus 102, 107-116.

Hiroi, T., Pieters, C. M., Takeda, H., 1994. Grain size of the surface regolith of asteroid 4 Vesta estimated from its reflectance spectrum in comparison with HED meteorites. Meteoritics 29, 394-396.

Hiroi, T., Binzel, R. P., Sunshine, J. M., Pieters, C. M., Takeda, H., 1995. Grain sizes and mineral compositions of surface regoliths of Vesta-like as-

teroids. Icarus 115, 374-386.

Kelley, M. S., Vilas, F., Gaffey, M. J., Abell, P. A., 2003. Quantified mineralogical evidence for a common origin of 1929 Kollaa with 4 Vesta and the HED meteorites. Icarus 165, 215-218.

Lawrence, S. J. and Lucey, P. G., 2007. Radiative Transfer Mixing Models of Meteoritic Assemblages. JGR 112, E07005.

Lazzaro, D. and 9 co-authors. 2000. Discovery of a Basaltic Asteroid in the Outer Main Belt. Science 288, 2033-2035.

Lazarro, D., Angeli, C. A., Carvano, J. M., Mothe-Diniz, T., Duffard, R., Florczak, M. 2004. S^3OS^2: the visible spectroscopic survey of 820 asteroids. Icarus 172, 179-220.

Lim, L. F., McConnochie, T. H., Bell, J. F., Hayward, T. L., 2005. Thermal infrared (8-13μm) spectra of 29 asteroids: the Cornell Mid-Infrared Asteroid Spectroscopy (MIDAS) Survey. Icarus 173, 385-408.

Lim, L. F., Emery, J. P, Moskovitz, N. A., 2009. Diogenite-like features in the Spitzer IRS (5-35 μm) spectrum of 956 Elisa. 40th Annual Lunar and Planetary Science Conference, The Woodlands, Texas, abstract no.2204.

Lodders, K., Fegley, B. 1997. The planetary scientist's companion. Oxford University Press, New York, USA.

Masiero, J., Hartzell, C., Scheeres, D. J., 2009. The effect of dust size distribution on asteroid polarization. Astronomical J. 138, 1557-1562.

McCord, T. B., Adams, J. B., Johnson, T. V., 1970. Asteroid Vesta: Spectral Reflectivity ad Compositional Implications. Science 168, 1445-1447.

Michtchenko, T. A., Lazzaro, D., Feraz-Mello, S., Roig, F., 2002. Origin of the basaltic asteroid 1459 Magnya: A dynamical and mineralogical study of the outer main belt. Icarus 158, 343-359.

Moroz, L., Schade, U., Wäsch, R., 2000. Reflectance spectra of olivine-orthopyroxene-bearing assemblages at decreased temperatures: Implications for remote sense of asteroids. Icarus 147, 79-93.

Moskovitz, N. A., Jedicke, R., Gaidos, E., Willman, M., Nesvorný, D., Fevig, R., Ivezić, Ž., 2008a. The distribution of basaltic asteroids in the main belt. Icarus 198, 77-90.

Moskovitz, N. A., Lawrence, S., Jedicke, R., Willman, M., Haghighipour, N., Bus, S. J., Gaidos, E., 2008b. A Spectroscopically Unique Main Belt Asteroid: 10537 (1991 RY16). ApJ Letters, 682, L57-L60.

Nesvorný, D., Jedicke, R., Whiteley, R. J., Ivezić, Ž., 2005. Evidence for Asteroid Space Weathering from the Sloan Digital Sky Survey. Icarus 173, 132-152.

Nesvorný, D., Roig, F., Gladman, B., Lazzaro, D., Carruba, V., Mothe-Diniz, T., 2008. Fugitives from the Vesta Family. Icarus 193, 85-95.

Parker, A., Ivezić, Ž., Jurić, M., Lupton, R., Sekora, M. D., Kowalski, A., 2008. The size distributions of asteroid families in the SDSS Moving Object Catalog 4. Icarus 198, 138-155.

Pieters, C. M., Hiroi, T., 2004. RELAB (Reflectance Experiment Laboratory): A NASA multiuser spectroscopy facility. 35th Annual Lunar and Planetary

Science Conference, League City, Texas, abstract no.1720.

Pieters, C. M., Binzel, R. P., Bogard, D., Hiroi, T., Mittlefehldt, D. W., Nyquist, L., Rivkin, A., Takeda, H., 2006. Asteroid-meteorite links: the Vesta conundrum(s). In: Lazzaro, D., Ferraz-Mello, S., Angel, F. J. (Eds.), Asteroid, Comets, Meteors. Vol. 228 of IAU Symposium. pp. 273-288.

Rayner, J. T., Toomey, D. W., Onaka, P. M., Denault, A. J., Stahlberger, W. E., Vacca, W. D., Cushing, M. C., Wang, S., 2003. SpeX: A Medium-Resolution 0.8-5.5 micron Spectrograph and Imager for the NASA Infrared Telescope Facility. PASP 115, 362.

Roig, F., Nesvorný, D., Gil-Hutton, R., Lazzaro, D., 2008. V-type Asteroids in the MIddle Main Belt. Icarus 194, 125-136.

Russell, C. T. and 20 co-authors, 2004. Dawn: A journey in space and time. Planet. Space Sci. 52, 465-489.

Ruzicka, A., Snyder, G. A., Taylor, L. A. 1997. Vesta as the HED parent body: Implications for the size of a core and large-scale differentiation. Met. Planet. Sci. 32, 825-840.

Scott, E. R. D., Greenwood, R. C., Franchi, I. A., Sanders, I. S., 2009. Oxygen isotopic constraints on the origin and parent bodies of eucrites, howardites and diogenites. 40th Annual Lunar and Planetary Science Conference, League City, Texas, abstract no. 2263.

Shkuratov, Y., Starukhina, L., Hoffmann, H., Arnold, G., 1999. A model of spectral albedo of particulate surfaces: Implications for optical properties of the Moon. Icarus 137, 235-246.

Storm, S., Bus, S. J., Binzel, R. P., 2007. Olivine-pyroxene distribution of S-type asteroids in the main belt. In: Bulletin of the American Astronomical Society. Vol. 38, p. 448.

Sunshine, J. M., Pieters, C. M., Pratt, S. F., 1990. Deconvolution of mienral absorption bands - An improved approach. J. Geophys. Res. 95, 6955-6966.

Tedesco, E. F., Noah, P. V., Noah, M., Price, S. D., 2004. IRAS Minor Planet Survey V6.0. NASA Planetary Data System, IRAS-A-FPA-3-RDR-IMPS-V6.0.

Thomas, P. C., Binzel, R. P., Gaffey, M. J., Storrs, A. D., Wells, E. D., Zellner, B. H. 1997. Impact Excavation on Asteroid 4 Vesta: Hubble Space Telescope Results. Science 277, 1492-1495.

Ueda, Y., Hiroi, T., Pieters, C. M., Miyamoto, M., 2002. Changes of Band I center and Band II/Band I area ratio in reflectance spectra of olivine-pyroxene mixtures due to the space weathering and grain size effects. 33rd Annual Lunar and Planetary Science Conference, League City, Texas, abstract no. 2023.

Vernazza, P., Brunetto, R., Strazzulla, G., Fulchignoni, M., Rochette, P., Meyer-Vernet, N., Zouganelis, I., 2006. Asteroid colors: a novel tool for magnetic field detection? The case of Vesta. Astron. Astrophys. 451, L43-L46.

Wasson, J. T., Pieters, C. M., Fisenko, A. V., Semjonova, L. F., Moroz, L. V., Warren, P. H., 1997. Simulation of space weathering of HED meteorites by laser impulse irradiation. 28th Annual Lunar and Planetary Science Con-

ference, League City, Texas, abstract no. 1505.

Wasson, J. T., Pieters, C. M., Fisenko, A. V., Semjonova, L. F., Warren, P. H., 1998. Simulation of space weathering of eucrites by laser impulse irradiation. 29th Annual Lunar and Planetary Science Conference, League City, Texas, abstract no. 1940.

Wetherill, G. W., Chapman, C. R. 1988. Asteroids and Meteorites. In: Kerridge, J. F., Matthews, M. S. (Eds.), Meteorites and the Early Solar System, Univ. of Arizona Press, Tucson, pp. 35-67.

Willman, M., Jedicke, R., Nesvorný, D., Moskovitz, N., Ivezić, Ž., Fevig, R., 2008. Redetermination of the space weathering rate using spectra of Iannini asteroid family members. Icarus 195, 663-673.

Xu, S., Binzel, R. P., Burbine, T. H., Bus, S. J., 1995. Small Main-Belt Asteroid Spectroscopic Survey: Initial Results. Icarus 115, 1-35.

Zappala, V., Cellino, A., Dell'oro, A., Migliorini, F., Paolicchi, P., 1996. Reconstructing the Original Ejection Velocity Fields of Asteroid Families. Icarus 124, 156-180.

Object	UT Date	Heliocentric Distance (AU)	Phase (deg)	Mag.	t_{exp} (min)
4 Vesta	Feb. 18-20, 1981[a]	2.38	4.0	6.12	–
	Oct. 9, 2000	2.26	25.9	7.3	10
809 Lundia	Aug. 26, 2008	1.93	23.9	14.6	8
956 Elisa	Jul. 5, 2008	1.85	16.6	14.6	16
	Oct. 9, 2008	1.85	16.9	15.7	88
1468 Zomba	Sep. 30, 2003	1.60	38.3		
	Apr. 26, 2009	2.51	13.0	17.4	80
1929 Kollaa	Feb. 19, 2001	2.21	14.4	15.3	24
2045 Peking	Jan. 14, 2002	2.48	21.7	16.7	40
	Aug. 26, 2008	2.50	16.9	16.2	87
2371 Dimitrov	Aug. 1, 2009	2.47	19.6	16.7	40
2442 Corbett	Sep. 30, 2003	2.25	7.8		
2511 Patterson	May 7, 2004	2.23	21.2	16.1	32
2566 Kirghizia	May 8, 2002	2.41	9.8	16.0	32
2579 Spartacus	Oct. 10, 2000	2.22	18.9	16.4	28
2653 Principia	Nov. 26, 2002	2.53	17.8	16.3	48
	Jul. 16, 2005	2.59	3.1	15.5	28
	Apr. 19, 2008	2.29	12.3	15.3	12
2763 Jeans	Jun. 26, 2004	2.24	12.6	15.7	32
	Jul. 5, 2008	1.99	12.2	14.9	16
	Aug. 26, 2008	1.92	17.3	14.9	24
2795 Lepage	Apr. 9, 2005	2.26	4.7	15.9	24
2823 van der Laan	Nov. 22, 2005	2.20	16.1		
2851 Harbin	Aug. 24, 2001	2.42	8.7	15.6	28
	Jan. 12, 2003	2.20	16.0	15.9	48
2912 Lapalma	Feb. 20, 2001	2.14	8.7	15.3	32
3155 Lee	Jun. 22, 2001	2.56	8.4	16.2	28

	Jul. 14, 2005	2.43	7.9	15.9	28
3657 Ermolova	Aug. 1, 2009	2.18	25.4	16.6	40
3703 Volkonskaya	Jun. 3, 2006	2.25	9.8		
3782 Celle	Nov. 26, 2002	2.60	17.1	16.8	32
	Jun. 25, 2004	2.19	13.3	15.5	28
4038 Kristina	Oct. 28, 2002	2.08	10.3		
4188 Kitezh	Aug. 14, 2001	2.10	10.8	15.3	28
4215 Kamo	Nov. 11, 2002	2.52	17.3	16.5	64
	Jul. 15, 2005	2.51	3.2	15.6	40
	Apr. 19, 2008	2.29	9.5	15.4	12
	Aug. 1, 2009	2.55	7.8	15.9	20
4796 Lewis	Jan. 9, 2009	2.46	13.9	17.0	33
5111 Jacliff	Sep. 5, 2005	2.06	7.6		
5481 Kiuchi	Aug. 1, 2009	2.37	10.5	16.3	54
5498 Gustafsson	Aug. 26, 2008	1.92	7.8	16.3	93
7800 Zhongkeyuan	Jan. 9, 2009	2.51	2.8	17.1	27
9481 Menchu	Aug. 26, 2008	2.48	6.1	17.3	40
9553 Colas	Jan. 8, 2009	1.99	20.3	17.4	120
16416 (1987 SM3)	Nov. 23, 2007	2.40	6.0	16.9	64
26886 (1994 TJ2)	Jul. 5, 2008	2.09	10.9	17.2	40
27343 (2000 CT102)	Aug. 26, 2008	1.94	11.7	16.6	48
33881 (2000 JK66)	Nov. 23, 2007	1.77	23.3	16.6	48
36412 (2000 OP49)	Nov. 23, 2007	2.12	11.8	16.9	40
38070 (1999 GG2)	Oct. 5, 2006	1.90	4.1	16.9	32
50098 (2000 AG98)	Sep. 4, 2005	1.94	11.4		
97276 (1999 XC143)	Nov. 23, 2007	2.05	2.4	16.6	56

Table 1: Summary of NIR Spectroscopic Observations
The columns in this table are: object number and designation, UT date of observation, heliocentric distance at the time of observation, the phase angle of the target, V-band magnitude of the target from the JPL HORIZONS system on the date of observation and net exposure time in minutes.
[a]Data from Gaffey (1997)

Object	Heliocentric Distance (AU)	Mean Surface Temp. (K)	BI Center (μm)	BI Slope	ΔBII (μm)	BII Center (μm)	BAR
4 Vesta	2.26	173.9	0.935	0.311	0.022	1.986	2.346
	2.38	169.4	0.943	0.090	0.023	2.003	2.436
809 Lundia	1.93	188.1	0.937	1.093	0.020	1.954	2.622
956 Elisa	1.85	192.2	0.932	0.963	0.019	1.964	2.707
	1.85	192.2	0.931	1.013	0.019	1.940	2.856
1468 Zomba	1.60	206.6	——	——	0.016	1.992	——
	2.51	165.0	0.938	0.902	0.024	2.001	2.187
1929 Kollaa	2.21	175.8	0.941	0.942	0.022	1.980	2.268
2045 Peking	2.48	166.0	0.938	0.861	0.024	1.976	2.430
	2.50	165.3	0.938	0.889	0.024	1.968	2.383
2371 Dimitrov	2.47	166.3	0.936	0.968	0.024	2.008	2.397
2442 Corbett	2.25	174.2	0.933	0.812	0.022	1.962	2.517
2511 Patterson	2.23	175.0	0.933	0.785	0.022	1.977	2.346
2566 Kirghizia	2.41	168.4	0.939	0.583	0.023	1.989	2.093
2579 Spartacus	2.22	175.4	0.935	0.516	0.022	2.011	1.383
	2.13	179.1	0.952	0.907	0.021	2.045	1.246
2653 Principia	2.55[a]	163.7	0.932	0.608	0.024	1.994	1.952
	2.29	172.7	0.940	0.742	0.022	2.012	1.934
2763 Jeans	2.24	174.6	0.944	0.664	0.022	2.019	1.985
	1.99	185.3	0.941	0.792	0.020	1.994	2.229
	1.92	188.6	0.942	0.898	0.020	2.027	2.255
2795 Lepage	2.26	173.9	0.938	0.532	0.022	1.973	2.234
2823 van der Laan	2.20	176.2	——	——	0.022	1.989	——
2851 Harbin	2.28[a]	173.1	0.922	0.693	0.022	1.934	2.363
2912 Lapalma	2.14	178.7	0.930	0.930	0.021	1.951	2.369
3155 Lee	2.49[a]	165.6	0.919	0.823	0.024	1.933	2.706
3657 Ermolova	2.18	177.0	0.931	0.703	0.022	1.942	2.406
3703 Volkonskaya	2.25	174.2	——	——	0.022	1.964	——
3782 Celle	2.40[a]	168.7	0.935	0.546	0.023	1.966	2.042
4038 Kristina	2.08	181.2	0.919	0.608	0.021	1.984	2.559
4188 Kitezh	2.10	180.4	0.939	0.777	0.021	1.979	2.009
4215 Kamo	2.52[a]	164.6	0.925	0.337	0.024	1.988	1.867
	2.29	172.7	0.932	0.372	0.022	1.975	2.061
	2.55	163.7	0.926	0.629	0.024	1.977	1.890
4796 Lewis	2.46	166.6	0.935	0.732	0.024	1.968	2.116
5111 Jacliff	2.06	182.1	0.926	0.558	0.021	1.964	2.259
5481 Kiuchi	2.37	169.8	0.932	0.922	0.023	1.959	2.550
5498 Gustafsson	1.92	188.6	0.941	0.986	0.020	1.990	2.470
7800 Zhongkeyuan	2.51	165.0	0.939	0.902	0.024	1.962	2.083
9481 Menchu	2.48	166.0	0.940	0.296	0.024	1.958	2.237
9553 Colas	1.99	185.3	0.932	0.803	0.020	1.949	2.387
16416 (1987 SM3)	2.40	168.7	0.939	0.887	0.023	1.988	2.155

26886 (1994 TJ2)	2.09	180.8	0.922	0.877	0.021	1.923	2.763
27343 (2000 CT102)	1.94	187.7	0.925	1.021	0.020	1.935	2.698
33881 (2000 JK66)	1.77	196.5	0.935	1.105	0.018	1.948	2.695
36412 (2000 OP49)	2.12	179.5	0.942	0.999	0.021	1.986	2.170
38070 (1999 GG2)	1.90	189.6	0.941	0.377	0.019	1.988	1.870
50098 (1999 AG98)	1.94	187.6	——	——	0.019	1.968	——
97276 (1999 XC143)	2.05	182.5	0.946	0.370	0.021	2.037	2.076

Table 2: Band Parameters of V-type Asteroids

The columns in this table are: object designation, heliocentric distance at the time of observation, estimated mean surface temperature (Eqn. 1), BI center, BI depth, temperature correction to BII center, BII center and the BII to BI area ratio (BAR). At the resolution of the spectra, the temperature correction for all of the BI centers is 0.002 μm. The band centers in this table have been temperature corrected. The maximum statistical errors (as determined from the spectrum of asteroid 2000 OP49) for these band parameters are: $\sigma_{BI} = 0.003$, $\sigma_{BII} = 0.011$ and $\sigma_{BAR} = 0.23$.

[a]Represents an average heliocentric distance from two separate observations.

Sample Info	BI Center (μm)	BI Area	BII Center (μm)	BII Area	BAR
Unaltered particulate	0.928	0.036	2.031	0.063	1.749
Moderately irradiated	0.934	0.026	2.015	0.058	2.188
Heavily irradiated	0.944	0.021	1.751	0.043	2.044

Table 3

Band Parameters for Eucrite Bereba

Sample Info	BI Center (μm)	BI Area	BII Center (μm)	BII Area	BAR
Unaltered particulate (grain size < 75 μm)	0.942	0.151	2.025	0.234	1.553
Partially irradiated (grain size < 75 μm)	0.942	0.144	2.023	0.229	1.586
Fully irradiated (grain size > 75 μm)	0.950	0.253	1.945	0.134	0.528

Table 4

Band Parameters for Eucrite Millbillillie

Spectral Parameter	Cell 2	Outside Cell 2	$i < 6°$	$i > 6°$
BI Center	0.939	0.935	0.939	0.932
BII Center	1.989	1.975	1.989	1.968
BAR	2.182	2.346	2.170	2.369

Table 5

Median Asteroidal Band Parameters

This table lists the median spectral parameters for four different dynamical regions. See the text for definitions of these regions. The maximum statistical errors (as determined from the spectrum of asteroid 2000 OP49) for these band parameters are: $\sigma_{BI} = 0.003$, $\sigma_{BII} = 0.011$ and $\sigma_{BAR} = 0.23$.

Sample Name	Type	Particle Size (μm)	BI Center (μm)	BII Center (μm)	BAR
Bialystok[a]	Howardite	150	0.937	1.990	1.6414
Binda	Howardite	25	0.928	1.948	1.6933
Bununu[a]	Howardite	25	0.928	1.951	1.4740
EET83376	Howardite	25	0.934	1.981	1.7840
EET87503	Howardite	25	0.929	1.970	1.6192
EET87513	Howardite	25	0.932	1.976	1.4692
Frankfort[a]	Howardite	25	0.927	1.945	1.7644
GRO95535	Howardite	25	0.929	1.963	1.6713
GRO95574	Howardite	125	0.929	1.953	1.7572
Kapoeta[a]	Howardite	25	0.928	1.936	1.3722
Le Teilleul[a]	Howardite	25	0.928	1.943	1.9352
Pavlovka[a]	Howardite	chip	0.921	1.934	1.9778
Petersburg[a]	Howardite	25	0.934	1.988	1.8304
QUE94200	Howardite	25	0.921	1.926	1.8620
QUE97001	Howardite	125	0.924	1.933	2.0792
Y7308	Howardite	25	0.927	1.942	1.6972
Y790727	Howardite	25	0.931	1.964	1.9103
Y791573	Howardite	25	0.926	1.948	1.8023
A87272	Eucrite	25	0.941	2.029	1.2244
A881819	Eucrite	25	0.931	1.976	1.5599
ALH78132	Eucrite	45	0.933	1.967	2.1383
ALH85001	Eucrite	25	0.925	1.952	1.5517
ALHA76005	Eucrite	25	0.935	1.996	1.7261
ALHA81001	Eucrite	45	0.937	2.024	2.7991
ALHA81011	Eucrite	125	0.951	2.042	1.3355
ALHA85001	Eucrite	1000	0.932	1.993	1.6795
Bereba[a]	Eucrite	25	0.941	2.023	1.7060

Bouvante	Eucrite	25	0.943	2.030	2.2411
BTN00300	Eucrite	45	0.947	2.029	0.9420
Cachari	Eucrite	25	0.940	2.027	1.4802
EET83251	Eucrite	1000	0.937	2.009	2.1906
EET87520	Eucrite	45	0.951	2.042	1.1116
EET87542	Eucrite	25	0.940	2.017	1.3458
EET90020	Eucrite	25	0.941	2.012	0.9865
EET92003	Eucrite	125	0.933	2.002	1.6588
EETA79005	Eucrite	25	0.934	1.974	2.0033
EETA79006	Eucrite	125	0.935	1.987	1.9342
EETA790B	Eucrite	1000	0.937	1.998	2.0071
GRO95533	Eucrite	25	0.941	2.040	1.4581
Ibitra[a]	Eucrite	25	0.940	2.000	1.1341
Jonzac[a]	Eucrite	25	0.939	2.013	1.7952
Juvinas[a]	Eucrite	25	0.936	2.003	1.6049
LEW85303	Eucrite	25	0.945	2.022	1.5695
LEW87004	Eucrite	25	0.934	1.963	1.7839
MAC02522	Eucrite	45	0.970	2.160	0.8309
MET01081	Eucrite	45	0.939	2.002	1.2518
Millbillillie[a]	Eucrite	25	0.938	2.019	1.3609
Moore County[a]	Eucrite	25	0.938	1.987	1.3885
NWA011	Eucrite	25	0.950	2.029	0.9193
Padvarninkai[a]	Eucrite	25	0.939	2.012	1.4851
Pasamonte[a]	Eucrite	25	0.939	2.003	1.5453
PCA82501	Eucrite	125	0.943	2.025	1.9056
PCA82502	Eucrite	25	0.941	2.025	2.2161
PCA91006	Eucrite	125	0.942	2.002	1.3592
PCA91007	Eucrite	125	0.943	2.042	2.1384
PCA91078	Eucrite	45	0.955	2.059	1.7840

Serra de Mage[a]	Eucrite	25	0.931	1.974	1.5117
Stannern[a]	Eucrite	25	0.938	2.017	1.9172
Y74450	Eucrite	25	0.934	1.970	1.3623
Y75011	Eucrite	1000	0.947	2.025	1.2378
Y791186	Eucrite	1000	0.949	2.052	1.4823
Y792510	Eucrite	25	0.942	2.032	1.3369
Y792769	Eucrite	25	0.941	2.026	1.6585
Y793591	Eucrite	25	0.939	2.011	1.8571
Y82082	Eucrite	25	0.947	2.034	1.6305
Y980318	Eucrite	75	0.940	2.016	1.4857
EETA79002	Diogenite	25	0.917	1.887	1.7581
Ellemeet[a]	Diogenite	25	0.920	1.901	1.9083
Johnstown[a]	Diogenite	25	0.914	1.874	1.5085
LAP91900	Diogenite	1000	0.925	1.920	1.9701
Roda[a]	Diogenite	chip	0.923	1.904	1.9880
Shalka[a]	Diogenite	chip	0.918	1.905	2.2039
Tatahouine[a]	Diogenite	chip	0.920	1.916	1.8623
Y74013	Diogenite	25	0.920	1.919	1.7630
Y75032	Diogenite	25	0.926	1.924	1.7040

Table 6: Band Parameters of HED Meteorites
[a] Indicates a fall rather than a find.
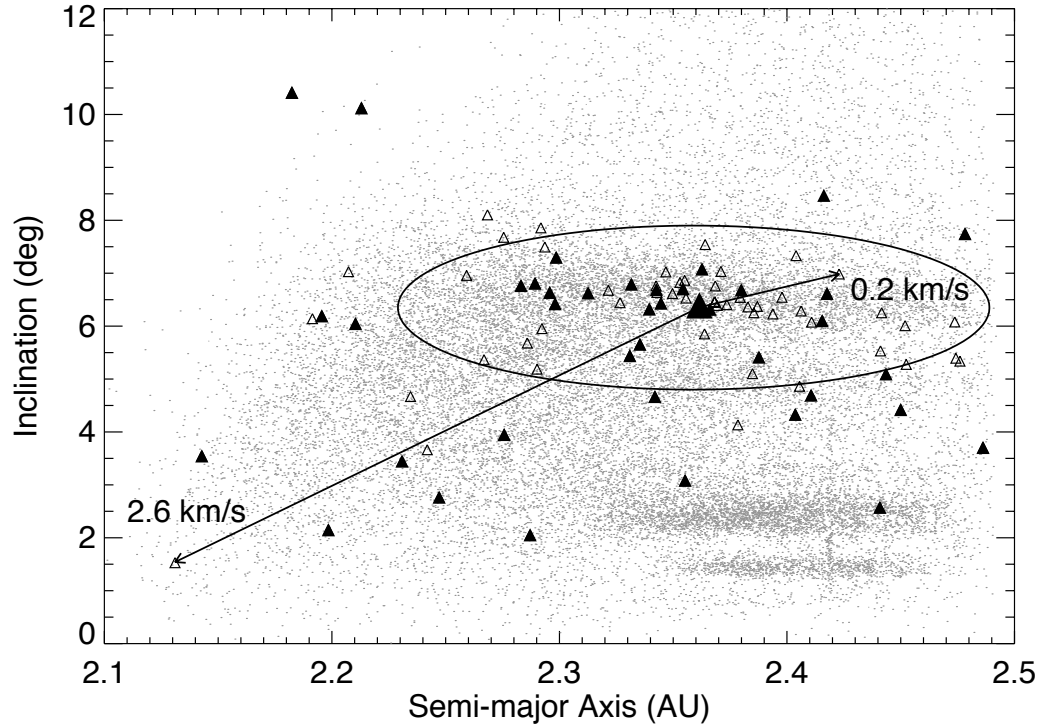
Fig. 1. Dynamical map in proper element space of V-type asteroids in the inner Main Belt. The filled triangles represent the V-type asteroids with NIR spectra included in this study. The open triangles are all spectroscopically confirmed V-types based solely on visible wavelength data (Xu et al., 1995; Bus and Binzel, 2002b; Lazzaro et al., 2004; Alvarez-Candal et al., 2006; Moskovitz et al., 2008a). Vesta is denoted by the large filled triangle at 2.36 AU, 6.35°. The grey dots in the background are all objects from the 4th release of the SDDS MOC (Parker et al., 2008). The ellipse traces the 0.6 km/s ejection velocity relative to Vesta. The relative ejection velocities for two objects are indicated by the arrows.

44
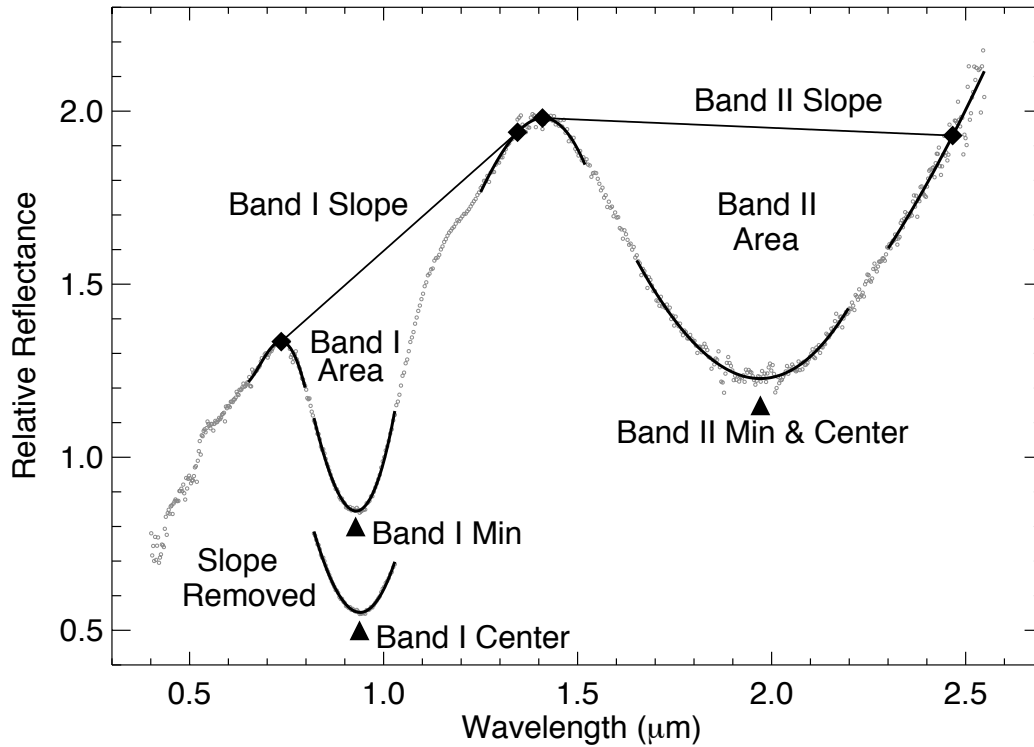
Fig. 2. Spectrum and band parameters of V-type asteroid 5498 Gustafsson. The data (grey circles) have been normalized to unity at 1.0 μm. The slope-removed data plot below the normalized spectrum. The band parameters of interest are denoted: Band I and II minima, centers, areas and slopes. This figure is based upon Cloutis et al. (1986). The filled diamonds mark the edges and tangent points for the Band I and II slopes. Note that all band parameters are defined relative to the fitted segments (solid black lines), not the data.
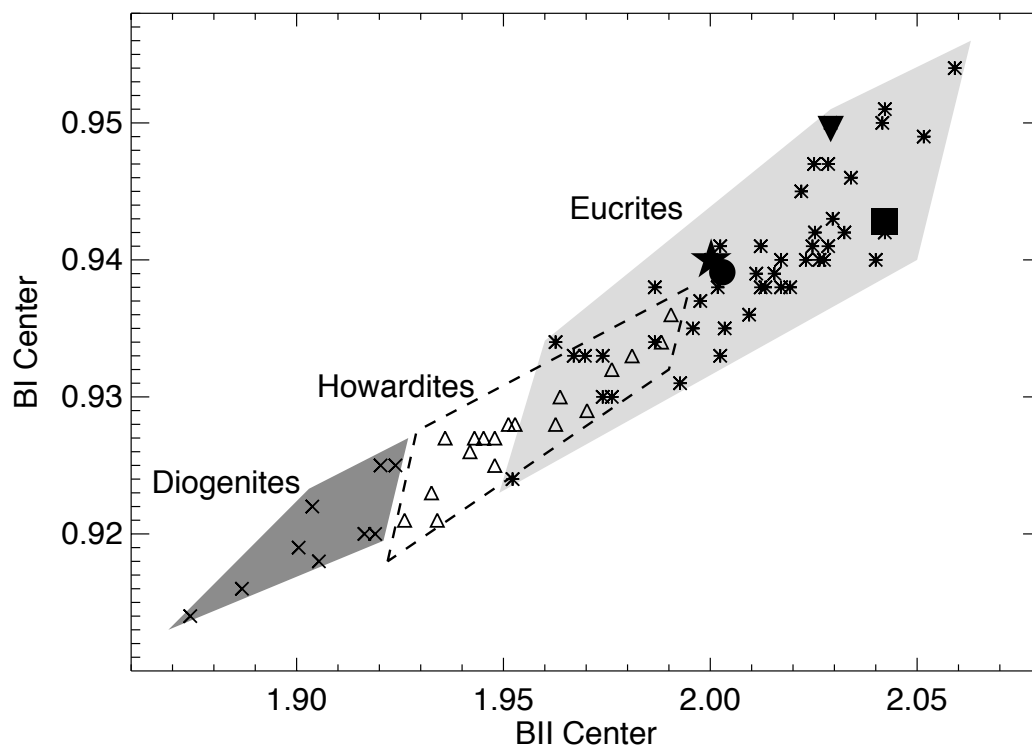
Fig. 3. Band centers of the howardites (triangles), eucrites (asterisks) and diogenites (×'s). Approximate boundaries for each of these subgroups are depicted as the dashed line, light grey and dark grey regions respectively. The eucrites and diogenites are very clearly segregated in this figure. The parameters of the four isotopically anomalous eucrites that are included in our study are denoted by the filled symbols: star (Ibitira), circle (Passamonte), upside-down triangle (NWA011), and square (PCA91007).
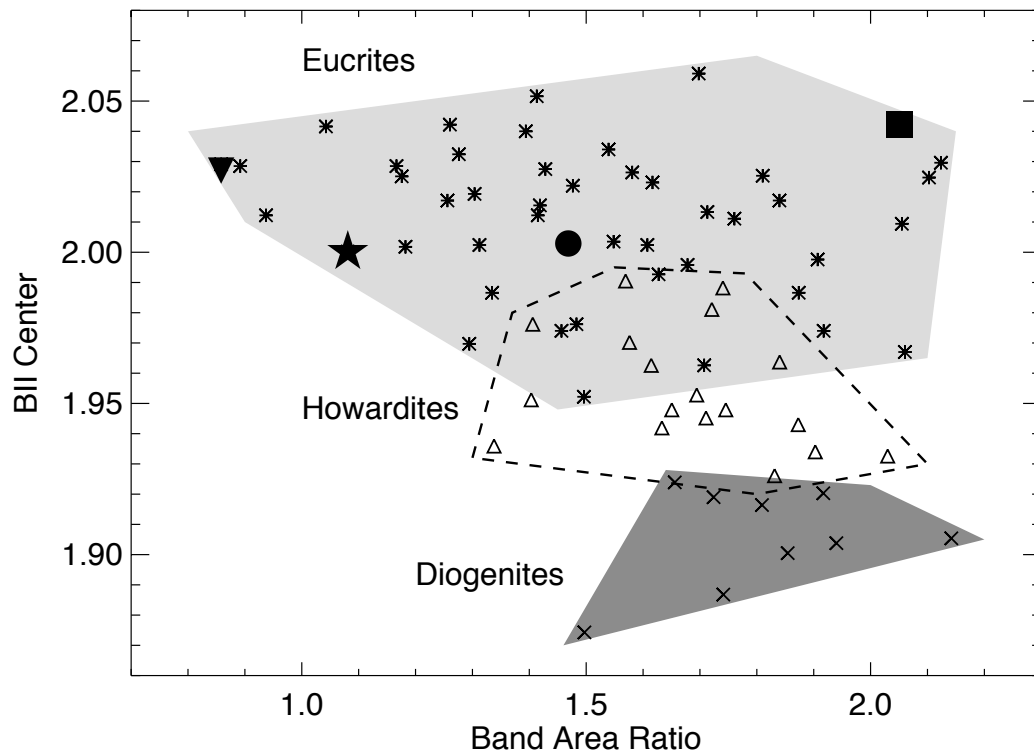
Fig. 4. BAR versus BII center for HED meteorites. The symbols and regions are the same as defined in Figure 3. The three HED subgroups are not clearly segregated in BAR, though diogenites do tend towards larger values.
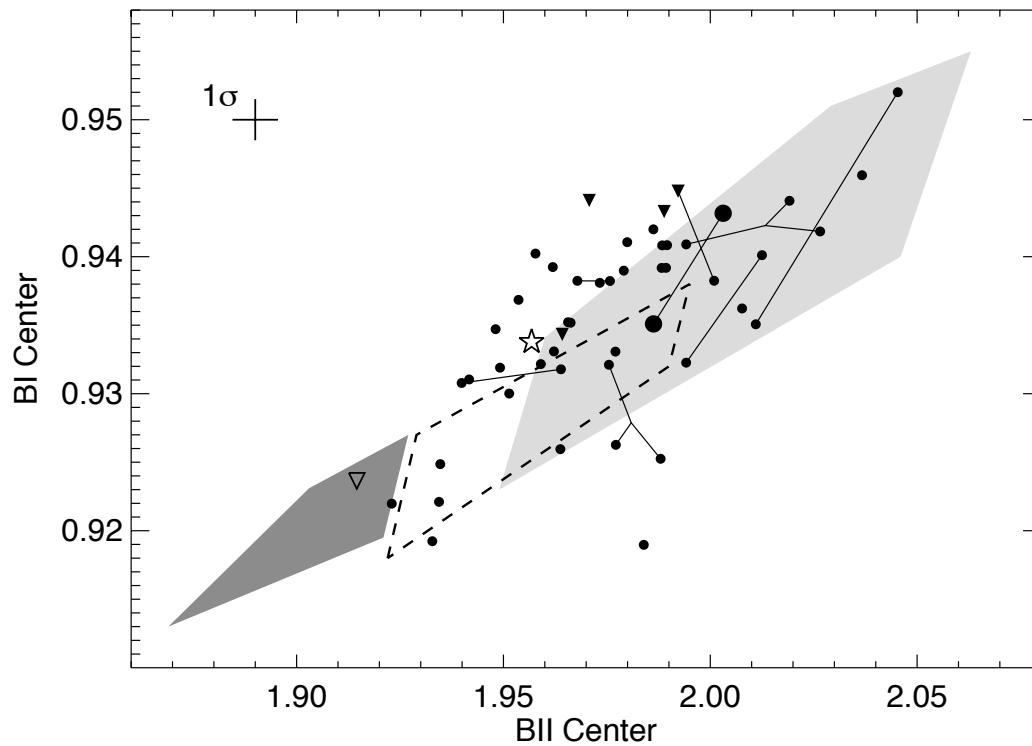
Fig. 5. Measured band centers of V-type asteroids (solid circles). Maximal 1-sigma error bars calculated from the analysis of the spectrum of 2000 OP49 (§4.3) are shown in the upper left corner. The approximate boundaries for each of the HED subgroups are the same as in Figure 3. Multiple observations of individual objects are connected by the thin lines. Vesta is plotted as the large filled circles. Upper limits to the BI centers for asteroids Zomba, Modena, Volkonskaya and 2000 AG98 are plotted as the upside-down filled triangles. The temperature-corrected band centers of non-Vestoid V-type Magnya (BI center = 0.934, BII center = 1.957) is plotted as a star. The Band II center and upper limit to the Band I center for non Vestoid V-type 1995 WV7 is plotted as an open upside-down triangle (lower left).
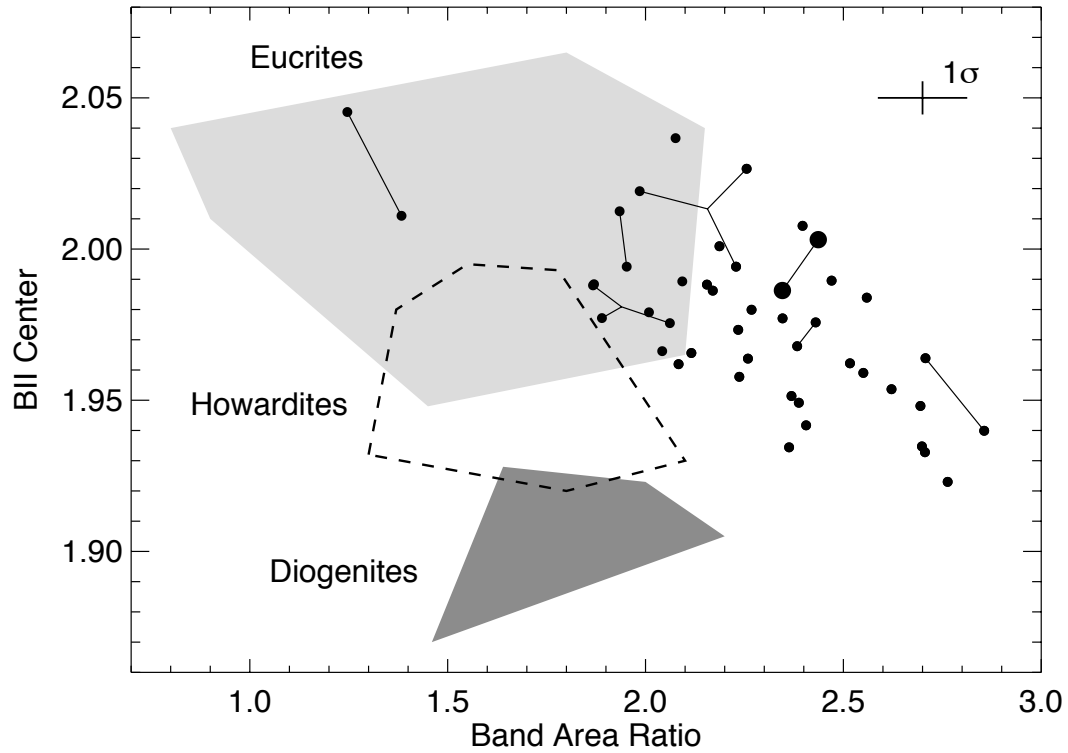
Fig. 6. BAR versus BII center for V-type asteroids. The maximum 1-sigma error bars that were calculated from the spectrum of 2000 OP49 are shown in the upper right corner. As in Figure 5 multiple observations are connected and Vesta is plotted as the large filled circle. The HED regions are the same as in Figure 4. Magnya plots off the right edge of this figure with a BII center = 1.93 and BAR = 3.39. The BARs of the V-type asteroids tend to be much larger than those represented by the HEDs.
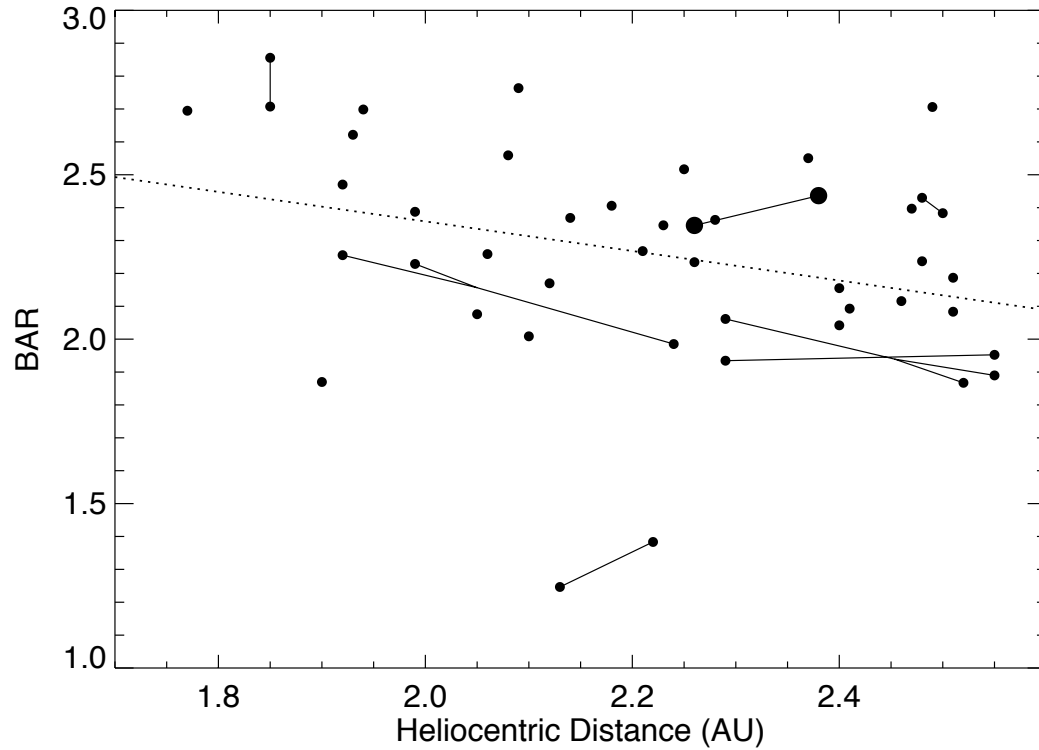
Fig. 7. Band area ratios versus heliocentric distance at the time of observation for our full set of V-type asteroids. Multiple observations are linked together. Vesta is plotted as the two large dots. This range of heliocentric distance corresponds to a temperature range of $\sim 160 - 200$ K. This figure shows a weak inverse correlation between BAR and surface temperature. The best fit (based on chi-square minimization) is indicated by the dotted line and is described by Eqn. 4.
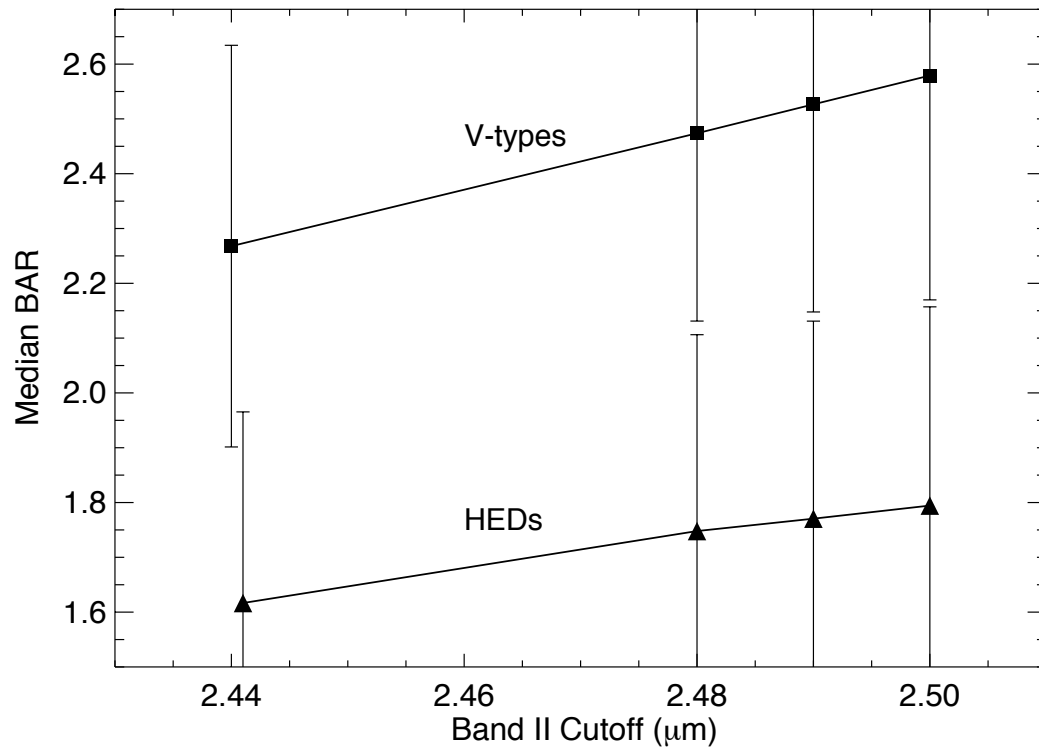
Fig. 8. Median BAR for V-type asteroids and HED meteorites as a function of the cutoff wavelength for the 2 μm absorption band. The vertical bars represent the standard deviations of the BARs. The data point at 2.44 μm for the HEDs has been horizontally offset for clarity.
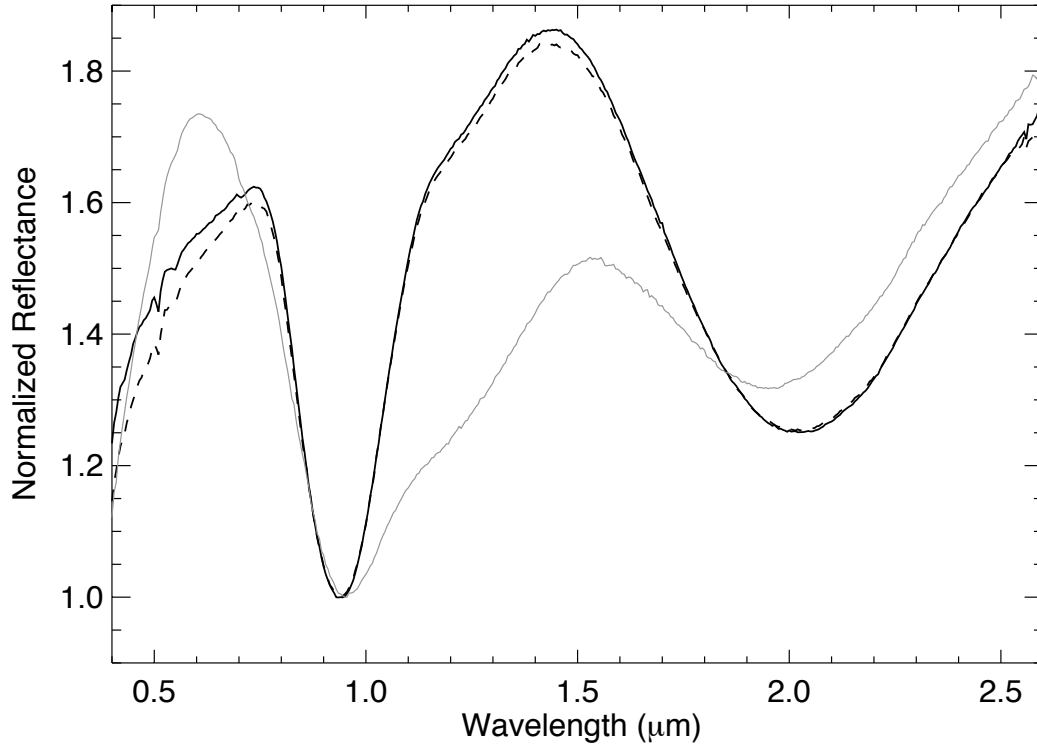
Fig. 9. Reflectance spectra of eucrite Millbillillie from the study of Wasson et al. (1998). The spectra have been normalized by the reflectance at the wavelengths of their respective Band I centers (Table 4) to emphasize the change in band parameters with irradiation level. The black line is the unaltered particulate sample (grain size < 75 μm). The dashed line is the partially irradiated material (grain size < 75 μm). The grey line is the spectrum of the fully irradiated material (grain size > 75 μm).
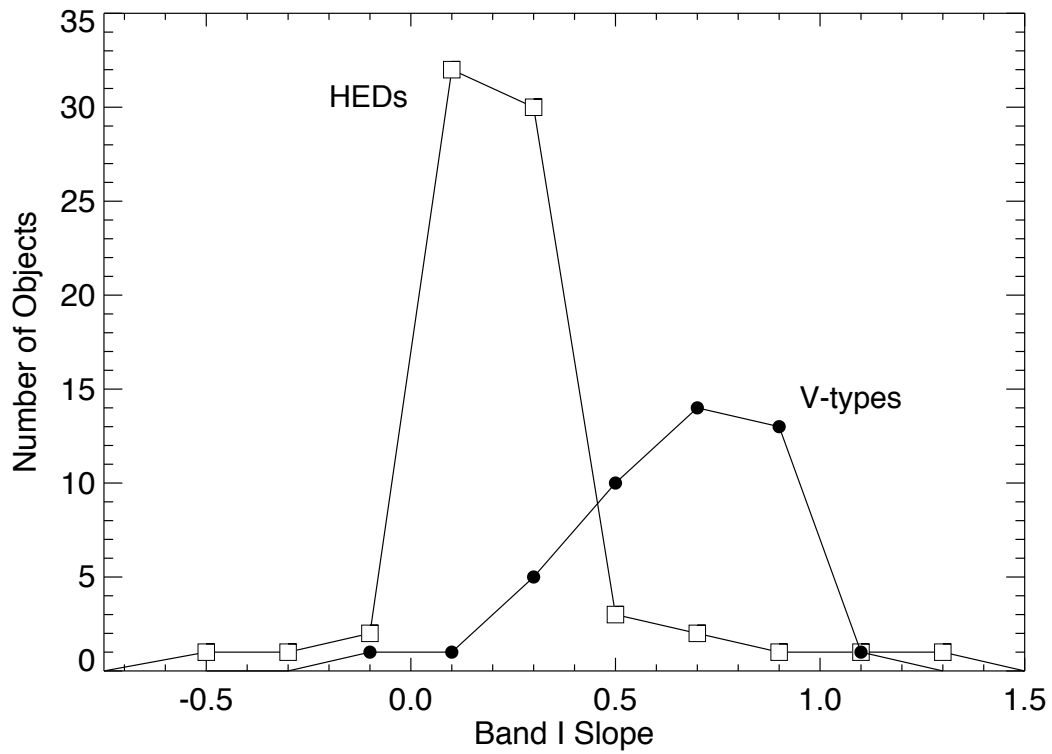
Fig. 10. Histograms of Band I slope for V-type asteroids and HED meteorites. The asteroids clearly have larger Band I slopes, consistent with the expected spectroscopic effects from the production of submicroscopic metallic iron by space weathering.
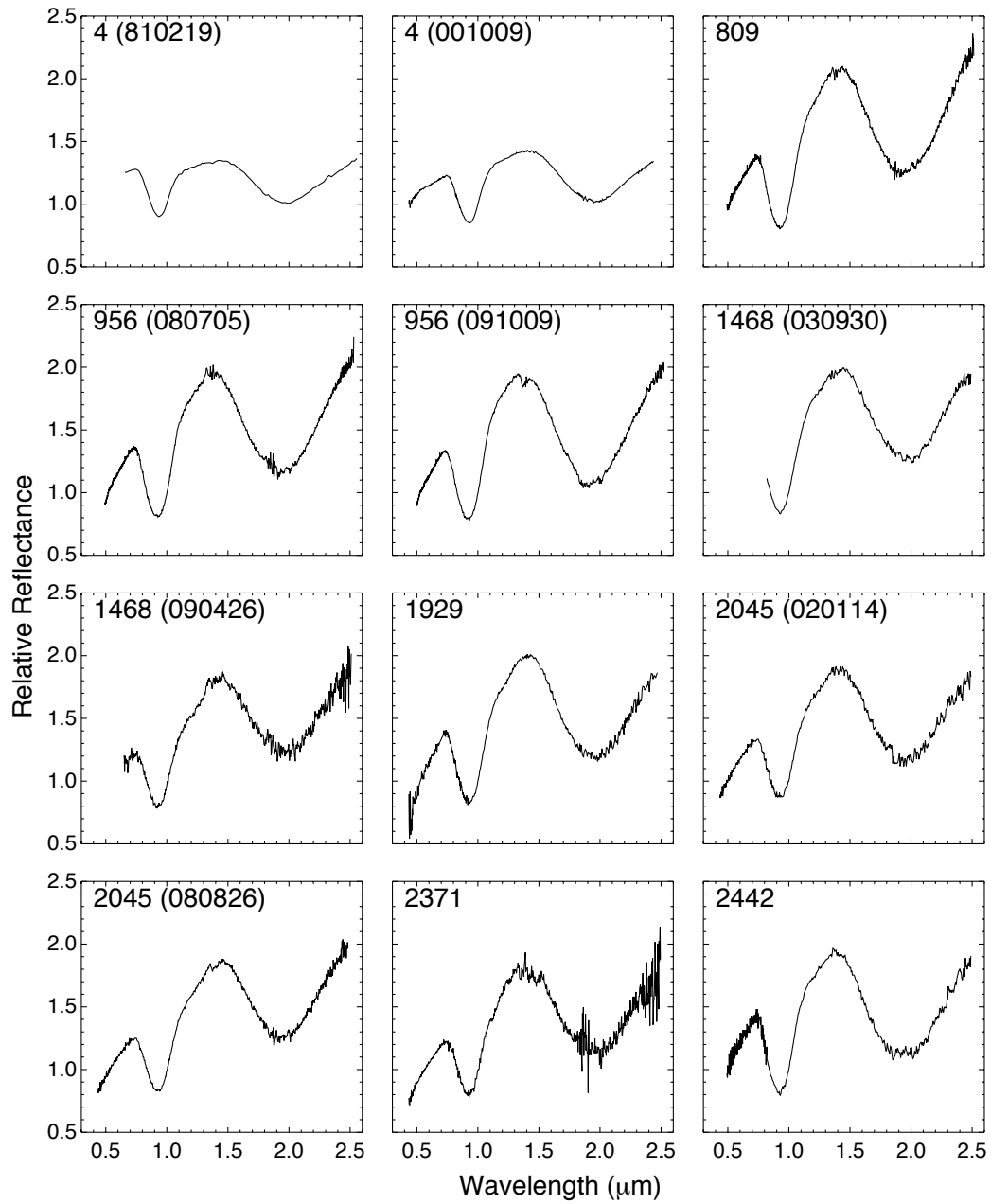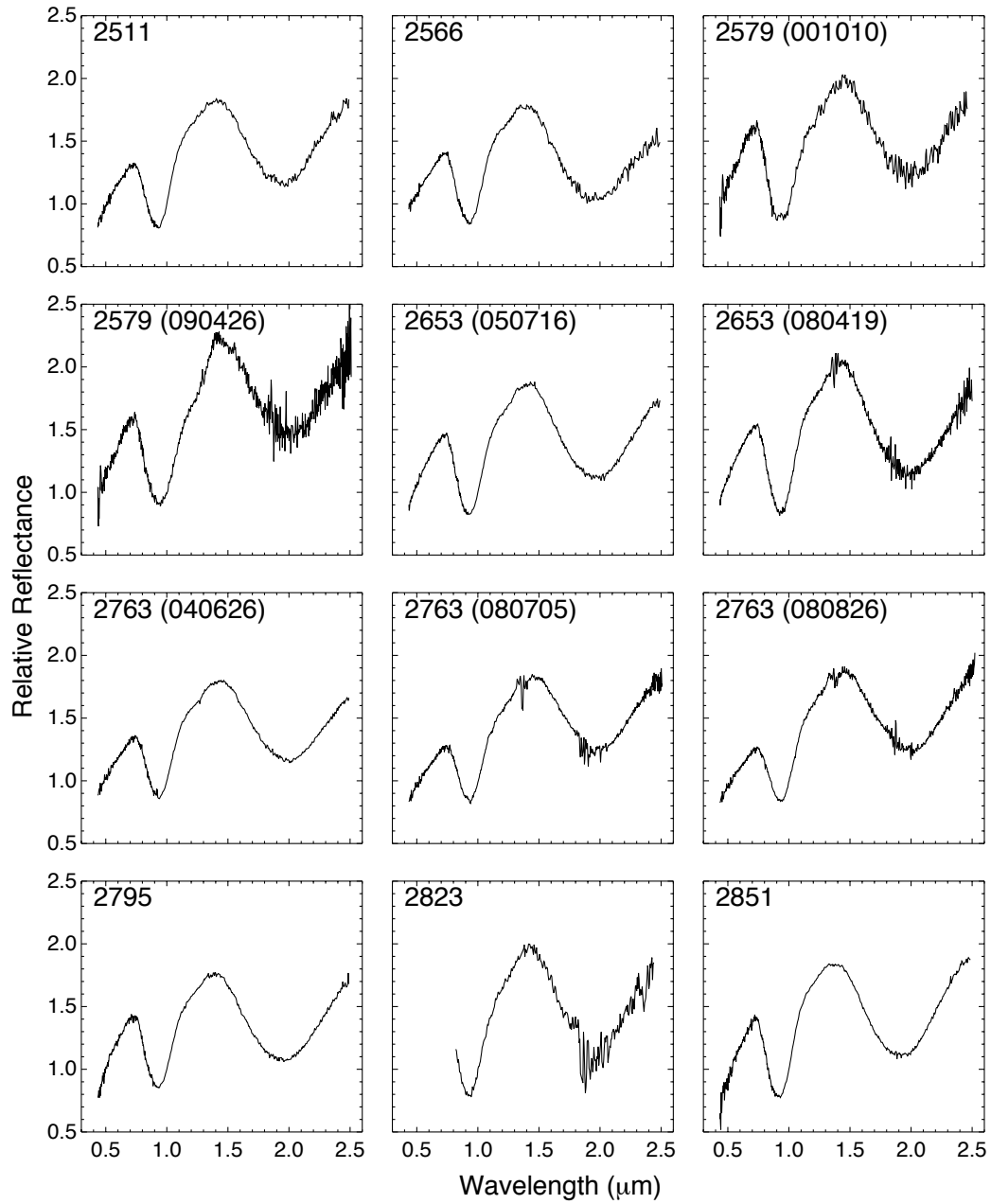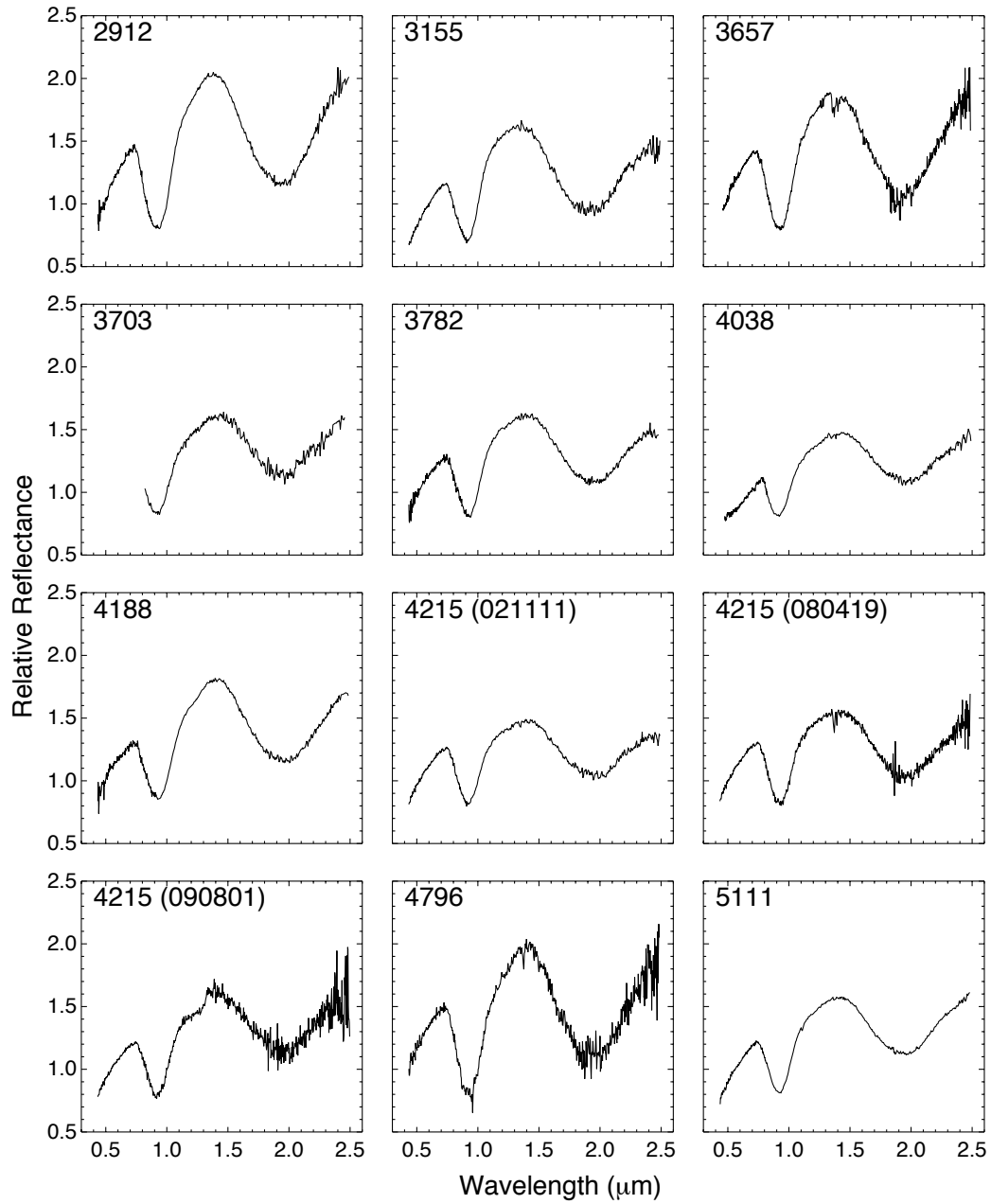
Fig. 11.

54
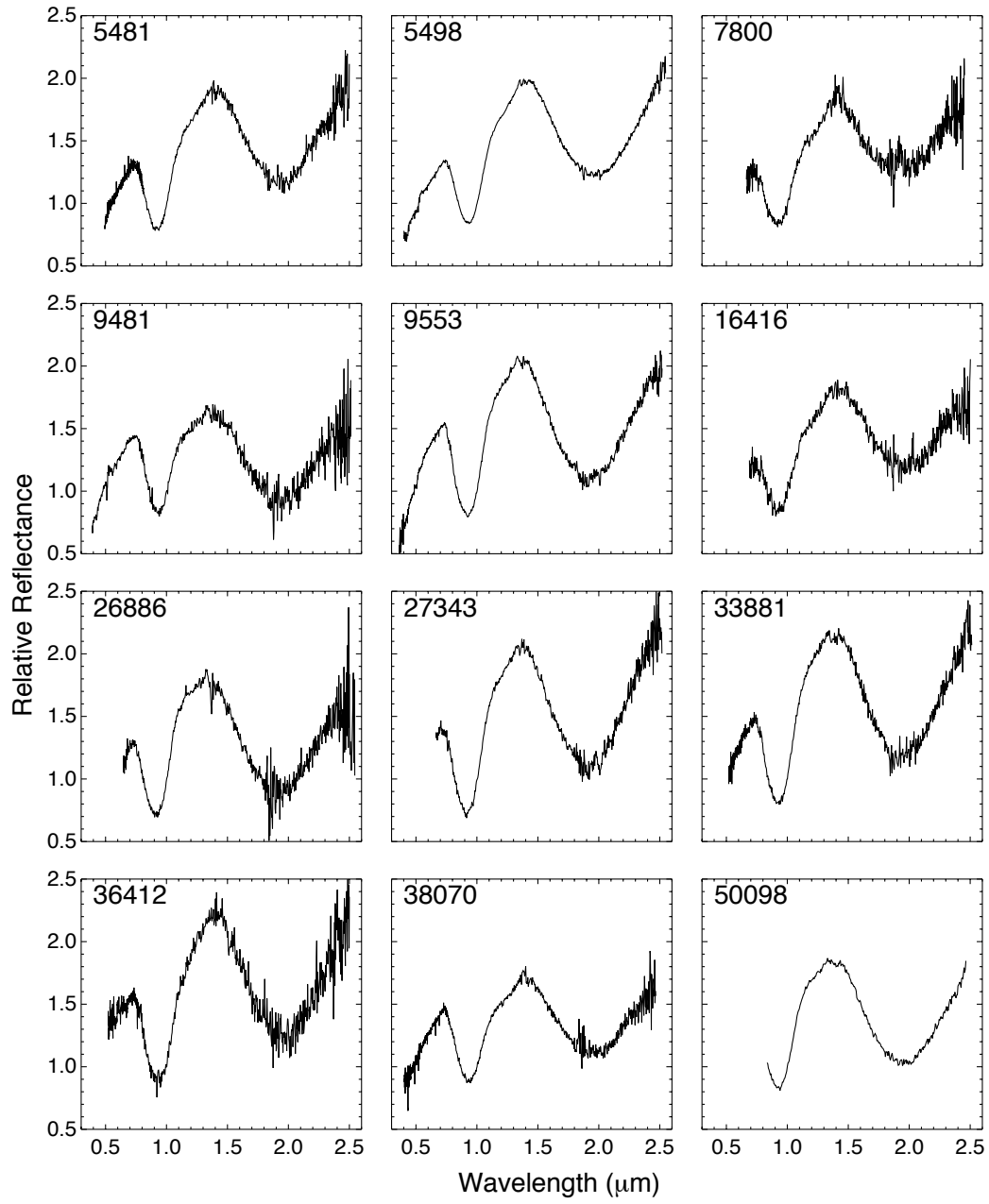
Figure 11 continued

Figure 11 continued

Figure 11 continued

2912
3155
3657
3703
3782
4038
4188
4215 (021111)
4215 (080419)
4215 (090801)
4796
5111

Relative Reflectance

Wavelength (μm)

Figure 11 continued

Figure 11 continued

97276

Relative Reflectance

Wavelength (μm)